

UNIVERSITY OF WOLLONGONG

DOCTORAL THESIS

Thesis Title

Author:

Supervisors:
Dr. Jenny FISHER, Prof. Clare
MURPHY

*A thesis submitted in fulfillment of the requirements
for the degree of Doctor of Philosophy
in the*

Centre of Atmospheric Chemistry
Chemistry Department 

June 7, 2019

Declaration of Authorship

I, Jesse GREENSLADE, declare that this thesis titled, "Thesis Title" and the work presented in it are my own. I confirm that:

- This work was done wholly or mainly while in candidature for a research degree at this University.
- Where any part of this thesis has previously been submitted for a degree or any other qualification at this University or any other institution, this has been clearly stated.
- Where I have consulted the published work of others, this is always clearly attributed.
- Where I have quoted from the work of others, the source is always given. With the exception of such quotations, this thesis is entirely my own work.
- I have acknowledged all main sources of help.
- Where the thesis is based on work done by myself jointly with others, I have made clear exactly what was done by others and what I have contributed myself.

Signed:

Date:

“Thanks to my solid academic training, today I can write hundreds of words on virtually any topic without possessing a shred of information, which is how I got a good job in journalism.”

Dave Barry

UNIVERSITY OF WOLLONGONG

Abstract

Science Medicine And Health

Chemistry Department

Doctor of Philosophy



Thesis Title

by Jesse GREENSLADE

Ozone in the troposphere is a toxic pollutant which causes respiratory and agricultural damage. The two main precursors are biogenic emissions of volatile organic compounds (BVOCs) and transport from the stratosphere. Most tropospheric ozone is formed through chemical reactions involving nitrogen oxides, the hydroxy radical, and volatile organic compounds (such as isoprene). Atmospheric chemistry transport models (CTMs) have uncertain BVOC emissions in Australia, affecting our ability to model and predict ozone production along with other important atmospheric processes. Isoprene, formaldehyde, and ozone in the troposphere are linked by oxidative chemistry and are all important to air quality, climate, and radiation budgets. My thesis has three aims: recalculating formaldehyde amounts over Australia seen by satellite using a global CTM (GEOS-Chem), determination of isoprene emissions using modelled formaldehyde yields along with satellite formaldehyde amounts, and attribution of ozone in the troposphere to chemical production and stratospheric transport. Model and observations are combined for each aim in this thesis.

To quantify isoprene emissions (the dominant BVOC), formaldehyde (one of the main products of isoprene oxidation) is used as a proxy. Formaldehyde observed by satellite over Australia is calculated based on modelled a priori vertical distributions using a CTM and a radiative transfer model. In order to compare satellite formaldehyde products against models or other measurements, corrections are required to remove the influence of the a priori profile. Impacts on formaldehyde levels from anthropogenic and pyrogenic sources are determined and filtered out to determine the biogenic footprint and minimise bias in isoprene emissions quantification.

Isoprene is predominantly emitted by trees and shrubs, and Eucalypts are potentially very high emitters. Subsequent oxidation reactions form formaldehyde which has a sufficiently long life in the atmosphere to establish chemical equilibrium. Using a simple linear model and assuming minimal transport and a chemical steady state allows an estimate of the yield of formaldehyde from isoprene emissions. This yield is modelled over Australia and then applied to the recalculated satellite formaldehyde to create a new estimate of Australian isoprene emissions. This technique is used to improve isoprene emissions estimates without the need for intensive measurement campaigns. Results are compared against existing measurement campaigns for validation and analysis. Isoprene emissions from Australian forests appear substantially lower than previous estimates have predicted.

The second most abundant source of tropospheric ozone is the stratosphere, which occasionally mixes into the troposphere bringing ozone-rich air masses down towards the earth's surface. Analysing the local weather patterns and ozone seasonality, most transport is seen to occur during low pressure frontal weather systems. This work provides a novel technique using a Fourier filter on ozone profiles for estimation and quantification of tropospheric ozone transported from the stratosphere. An estimate encompassing three measurement stations over the Southern Ocean near Australia of about 7.2×10^{17} molec cm⁻² per year is derived.

Overall, this work should improve the knowledge of tropospheric ozone and its precursors for Australia.

Acknowledgements

Thanks to my supervisor Jenny Fisher, the whole Atmospheric Chemistry team at Wollongong who made me feel at home: Beata, Clare Murphy, Dagmar, Doreena, Elise, Joel, Kaitlyn, Max, Nick Deutscher, Nicholas Jones, Ruhi, Stephen Wilson, and Voltaire.

Contents

<input type="checkbox"/>	Declaration of Authorship	iii
	Abstract	viii
	Acknowledgements	ix
1	Introduction and Literature Review	1
1.1	The atmosphere	1
1.1.1	Structure	1
1.1.2	Composition and chemistry	2
1.1.3	Radiative Forcing	3
1.2	Ozone	4
1.2.1	Stratospheric ozone	4
1.2.2	Tropospheric ozone	7
1.2.3	Stratosphere to troposphere transport	10
1.2.4	Chemical production	10
1.3	Volatile Organic Compounds	12
1.3.1	Emissions	13
1.3.2	Isoprene	14
1.3.3	Isoprene chemistry	15
1.3.3.1	Oxidation	17
1.3.3.2	High NO _x pathway	18
1.3.3.3	Low NO _x pathway	18
1.3.3.4	Night time processes	19
1.4	Formaldehyde	19
1.4.1	Sources and sinks	20
1.4.2	Measurement techniques	21
1.4.2.1	Satellite measurements	23
1.5	Atmospheric Chemistry Modelling	24
1.5.1	Box models	24
1.5.2	Chemical transport models	25
1.5.3	Emissions	26
1.5.4	Uncertainties	27
1.5.4.1	Emissions Inventories	27
1.5.4.2	Resolution	28
1.5.4.3	Chemistry mechanisms	28
1.5.4.4	Clouds	28
1.5.4.5	Soil Moisture	29
1.6	Australia and the southern hemisphere	29

1.6.1	Ozone	31
1.6.2	Biogenic VOCs	32
1.6.3	Measurements	33
1.7	Aims	33
2	Data and Modelling	35
2.1	Introduction	35
2.2	Datasets	36
2.2.1	Satellite	36
2.2.1.1	Formaldehyde	37
2.2.1.2	Nitrogen dioxide	38
2.2.1.3	Aerosol optical depth	40
2.2.1.4	Active fires	40
2.2.1.5	Carbon monoxide	40
2.2.1.6	Uncertainties	40
2.2.2	Model datasets	41
2.2.2.1	GEOS-Chem output	41
2.2.2.2	Meteorological reanalysis	41
2.2.2.3	Surface temperatures	42
2.2.3	Campaign datasets	42
2.2.3.1	Measurements of Urban, Marine and Biogenic Air (MUMBA)	42
2.2.3.2	Sydney Particle Studies (SPS1, SPS2)	45
2.2.3.3	Ozonesondes	47
2.2.3.4	Wollongong	47
2.2.3.5	Uncertainties	48
2.3	Satellite formaldehyde	50
2.3.1	Pixel filtering	52
2.3.2	DOAS	54
2.3.3	Air mass factor (AMF)	56
2.3.4	LIDORT	57
2.3.5	Uncertainty	57
2.4	GEOS-Chem	59
2.4.1	Overview	59
2.4.2	Installing and running GEOS-Chem	60
2.4.3	Chemical Mechanism	60
2.4.4	GEOS-Chem isoprene	62
2.4.4.1	Oxidation	63
2.4.4.2	Nitrogen oxide impacts	63
2.4.4.3	OH	64
2.4.5	Emissions from MEGAN	64
2.4.6	Nitrogen oxides	66
2.4.7	GEOS-Chem simulations	67
2.4.7.1	GEOS-Chem outputs	67
2.4.7.2	GEOS-Chem runs	71
2.4.7.3	UCX vs tropchem	72
2.5	Calculating new AMF	78
2.6	Recalculation of OMI HCHO	80

2.6.1	Outline	81
2.6.2	Creating new shape factors	82
2.6.3	Creating new AMF using GEOS-Chem	83
2.6.3.1	Updating shape factors	83
2.6.3.2	Recalculating the AMF using PP code	83
2.6.3.3	Saving the AMF with satellite pixels	84
2.6.4	Vertical columns from AMF	84
2.6.5	Reference sector correction	84
2.6.6	Corrected vertical columns	88
2.6.7	Binning the results daily	88
2.6.8	Difference between original and corrected OMI HCHO columns	90
2.7	Filtering Data	93
2.7.1	Pyrogenic filter	93
2.7.2	Anthropogenic filter	99
2.7.3	Smearing filter	104
2.7.3.1	Calculation of smearing	104
2.7.3.2	NO _x dependence	108
2.8	Relationship between temperature and HCHO	108
2.9	Process schematic	111
2.10	Data Access	117
3	Biogenic Isoprene emissions in Australia	121
3.1	Introduction	121
3.1.1	Aims	122
3.1.2	Existing emissions estimates	122
3.1.3	Top-down isoprene emissions estimates	123
3.1.3.1	Bayesian inversion	123
3.1.3.2	Linear inversion	124
3.2	Methods	125
3.2.1	Outline	125
3.2.2	Masks and reprocessed satellite HCHO	126
3.2.3	GEOS-Chem emissions	128
3.2.4	Relationship between isoprene emissions and formaldehyde	128
3.2.5	Calculation of modelled slope	130
3.2.6	Modelled background HCHO	132
3.2.7	Calculation of Emissions	132
3.2.8	Sensitivity to smearing	136
3.2.8.1	Modelled HCHO lifetimes	136
3.2.9	Running GEOS-Chem using a posteriori emissions	138
3.2.10	Conversion to emissions by kg	140
3.3	Results	140
3.3.1	A posteriori emissions	140
3.3.1.1	Diurnal emissions	147
3.3.1.2	Trends	148
3.3.2	Modelled impacts of reduced isoprene emissions	151
3.3.2.1	Implications for HCHO	151
3.3.2.2	Implications for ozone	151

3.3.3 Comparison with in situ measurements	158
3.4 Uncertainty	161
3.4.1 Top down emissions	163
3.4.2 Model Uncertainty	164
3.4.3 Satellite Uncertainty	168
3.4.4 Sensitivity to AMF recalculation	173
3.4.5 Sensitivity to filtering	173
3.5 Conclusions and implications	173
4 Stratospheric ozone intrusions	179
4.1 Foreword	179
4.2 Introduction	179
4.3 Data and Methods	181
4.3.1 Ozonesonde record in the Southern Ocean	181
4.3.2 Model description	185
4.3.3 Characterisation of STT events and associated fluxes	185
4.3.4 Biomass burning influence	187
4.3.5 Classifying synoptic conditions during STT events	188
4.4 STT event climatologies	189
4.5 Simulated ozone columns	192
4.6 Stratosphere-to-troposphere ozone flux from STT events	196
4.6.1 Method	196
4.6.2 Results	198
4.6.3 Comparison to literature	203
4.7 Sensitivities and limitations	204
4.7.1 Event detection	204
4.7.2 Flux calculations	204
4.8 Conclusions	206
4.9 Contributions and Acknowledgements	207
5 Summary and Concluding remarks	209
5.1 Outcomes	209
5.2 Isoprene emissions	210
5.3 Ozone over Australia	210
5.4 Outputs	211
5.5 Future work	214
Bibliography	217

List of Figures



1.1	Pressure (red) logarithmically decreasing, shown with percentage of atmosphere below at several points. Temperature (green) changes throughout the atmosphere. Figure edited from https://climate.ncsu.edu/edu/Structure	2
1.2	The overall radiative forcings and uncertainties of several atmospheric constituents This is an image taken from Forster et al. (2007), found at https://www.ipcc.ch/publications_and_data/ar4/wg1/en/faq-2-1.html	5
1.3	The overall radiative forcings and uncertainties of several atmospheric constituents This is an image taken from Stocker et al. (<i>IPCC, 2013: Climate Change 2013: The Physical Science Basis. Contribution of Working Group I to the Fifth Assessment Report of the Intergovernmental Panel on Climate Change</i>), chapter 8.	6
1.4	Tropospheric ozone processes, Figure 1 in Young et al. (2017). DOI: https://doi.org/10.1525/elementa.265.f1	8
1.5	Figure showing the NO - NO ₂ - ozone photoequilibrium cycle without and with (A, B respectively) influence from VOCs. Figure reproduced from Atkinson (2000).	9
1.6	Ozone production rate dependent on NO _x and VOC concentrations (Mazzuca et al. 2016).	11
1.7	Isoprene products following oxidation by OH, figure from Mao et al. (2013)	16
1.8	HCHO spectrum, with a typical band of wavelengths used for DOAS path measurements. This is a portion of an image from Davenport et al. (2015).	22
1.9	An example spectrum showing interferences used for species concentration measurements by GOME-2. Image by EUMETSAT and ESA (EUMETSAT 2015).	24
1.10	Standard box model parameters, image taken from Jacob (1999).	26
1.11	Forest types in Australia (http://www.agriculture.gov.au/abares/forestsaustralia/australias-forests)	30
1.12	Part of a figure from Guenther et al. (2006) showing global isoprene emission factors.	31
2.1	Example of NO ₂ tropospheric columns taken from the OMNO2d product.	38
2.2	Average 2005 tropospheric NO ₂ from OMNO2d with pixels screened for < 30% cloud cover.	39

2.3 CPC daily maximum temperature dataset output for 1, Jan, 2005.	42
2.4 Locations of VOC measurements (top panel) and ozonesonde release sites (bottom panel). Inlaid in top panel is the flight paths over Australia of the HIPPO campaign.	43
2.5 Top: MUMBA, SPS1, and SPS2 time-series for HCHO (orange) and isoprene (magenta), along with detection limits (dashed). Bottom: isoprene measurements superimposed onto a single year.	44
2.6 SPS HCHO (yellow) and isoprene (green) time series, along with detection limits (dashed). SPS 1 (left) took place in late summer 2011, while SPS 2 (right) occurred during autumn 2012.	46
2.7 Mean midday FTIR profile (x_{ret}) and a priori profile (x_{apri}). Shaded area shows the inter-quartile range over the same time period. Profile is averaged between November 2007 to April 2013.	48
2.8 Left panel shows the mean midday (13:00 - 14:00 local time) total column averaging kernel, along with the inter-quartile range (IQR) between November 2007 and April 2013. Right panel shows the mean averaging kernel for the vertical profile over the same time period, coloured by vertical level. One in six vertical levels are labelled and plotted with a solid line, the rest are shown with dashed lines. TODO: add x-axis label (Averaging kernal [unitless])	49
2.9 Figure 1 and Table 1 from Schenkeveld et al. (2017), with the following caption “An impression of OMI flying over the Earth. The spectrum of a ground pixel is projected on the wavelength dimension of the charge-coupled device (CCD; the columns). The cross-track ground pixels are projected on the swath dimension of the CCD (the rows). The forward speed of 7 km s^{-1} and an exposure time of 2 s lead to a ground pixel size of 13 km in the flight direction. The viewing angle of 114° leads to a swath width on the ground of 2600 km.” The table shows the optical properties for OMIs three channels.	51
2.10 Solar and viewing zenith angles, image copied from Wikipedia (2016), originally from a NASA website.	52
2.11 HCHO Column amount histograms for a subset of OMI swaths over Australia on the 18th of March 2013. Negative entries are shown in the left panel, positive in the right. Note the different scale between negative and positive panels. TODO: add x-axis label (molec cm^{-2}).	55
2.12 Top row shows $0.25^\circ \times 0.3125^\circ$ binned OMHCHO columns with one day, one month, and one month with non-biogenic masking applied from left to right respectively. Bottom row shows the uncertainty for each grid square after averaging. TODO: combine colour bars on top,bottom	58
2.13 MEGAN schematic, from http://lar.wsu.edu/megan/	65
2.14 Left to right columns show tropospheric NO_2 columns (Ω_{NO_2} ; molec cm^{-2}) from GEOS-Chem (GC), OMNO2d (OMI), and the differences. Each row shows one season from 2005, the left two columns use the left colour scale, while the third column uses the right colour scale.	68

2.15	Left and right columns show anthropogenic and soil emissions of NO respectively from GEOS-Chem in molec cm ⁻² s ⁻¹ . Each row shows one season from 2005. Anthropogenic and soil emissions use a logarithmic and linear colour scale respectively.	69
2.16	The first column shows the scatter plots of tropospheric NO ₂ columns between GEOS-Chem (y-axis) and OMNO2d (x-axis) at 2° × 2.5°. The reduced major axis linear regression is drawn in red, and the equation, regression coefficient (r), and number of grid squares (n) used is inlaid as a legend. The second and third columns show the scatter between emissions and the bias between GEOS-Chem and OMNO2d (GC-OMI), for anthropogenic and soil emissions respectively. These two columns share the far right axis; however, emissions are from anthropogenic and soil sources respectively. All scatter points are coloured by the sum of anthropogenic and soil NO emissions (from GEOS-chem), as per the colour bar shown at the bottom.	70
2.17	Surface HCHO simulated by GEOS-Chem with UCX (A: top left), and without UCX (B: top right), along with their absolute and relative differences (bottom left, right respectively). Amounts are the average of all times between 1 Jan and 28 Feb 2007.	73
2.18	As Figure 2.17 using total column amounts instead of surface concentrations.	74
2.19	As Figure 2.17, except showing isoprene surface concentrations.	75
2.20	As Figure 2.19, except showing isoprene total column amounts.	76
2.21	Total column ozone simulated by GEOS-Chem with UCX (A: top left), and without UCX (B: top right), along with their absolute and relative differences (bottom left, right respectively). Amounts are the average of all times between 1 Jan and 28 Feb 2007.	77
2.22	Top row: averaged OMI Satellite AMF for 2005, from the OMHCHO data set (left, AMF_{OMI}), recalculated using GEOS-Chem shape factors (middle, AMF_{GC}), and recalculated using GEOS-Chem shape factors and scattering weights (right, AMF_{PP}). Middle row: AMF time series over 2005 for each recalculation. Bottom row: AMF frequency distributions over January and February. Oceanic pixels are filtered out, only land pixels are included in this figure.	85
2.23	Example of remote Pacific RSC using 8-day average measurements and one month modelled data. <i>OMIVC</i> shows the uncorrected vertical columns, while <i>Corrected</i> shows the corrected vertical columns. OMI corrections shows the correction applied globally based on latitude and OMI track number(sensor). Ω_{GC} shows the GEOS-Chem modelled HCHO VC over the reference sector (region within black vertical lines), with Ω_{VCC} showing the corrected VC over the same area.	87
2.24	Example of track correction interpolations for January 1st 2005, points represent the difference between satellite slant column measurements and modelled slant columns over the remote Pacific.	89

2.25 Row 1: regridded corrected Ω_{HCHO} from OMHCHO on January 1, 2005: original (left), recalculated using new shape factors (middle), and additionally using updated scattering weights (right). Row 2: shows the monthly average for January 2005. Row 3: shows the distribution over the month for each of the three column amounts. Distribution bins are logarithmic, resulting in wider bins for higher column amounts.	91
2.26 Monthly pixel counts over Australia (non-oceanic) used in recalculations of vertical columns. N_{GC} refers to the number of pixels used in AMF recalculation without running code from Paul Palmer, N_{PP} refers to those which have been recalculated using their code. Filters applied are described in Section 2.7,	92
2.27 Top row: averaged OMI Satellite VCC for 2005, from the OMHCHO data set (left, VCC_{OMI}), recalculated using GEOS-Chem shape factors (middle, VCC_{GC}), and recalculated using GEOS-Chem shape factors and scattering weights (right, VCC_{PP}). Middle row: VCC time series over 2005 for each recalculation. Bottom row: VCC frequency distributions over January and February. Oceanic pixels are filtered out, only land pixels are included in this figure.	94
2.28 Top row shows grid squares filtered out by anthropogenic (left) and pyrogenic (right) influence masks over 2005. Bottom row shows portion of Australian grid squares filtered out each day.	95
2.29 Recalculated OMI vertical HCHO columns and pixel counts for January 2005. Column 1: VCC_{PP} amounts after applying the active fire filter. The filter is applied at $0.25^\circ \times 0.3125^\circ$ resolution, before output is averaged into $2^\circ \times 2.5^\circ$ bins. Column 2: Pixel counts after applying the active fire filter (summed into $0.25^\circ \times 0.3125^\circ$ bins). Row 1-4: increasing number of prior days which have active fires are included when masking fire influence. The first row shows the values without applying any active fire filter. The average and maximum VCC column amount (at $0.25^\circ \times 0.3125^\circ$ resolution), and number of pixels, is inset as text in column 1 of each row.	97
2.30 AAOD from OMAERUVd (columns 1, 2, 3) over Australia for four different scenarios (rows 1-4). Black Saturday (row 2) marks the occurrence of widespread bush fires across Victoria. The transported plume in row three can be seen in the overlaid AOD shown in the last column, Indonesia (northwards from Darwin) suffered from wide-spread forest fires around this time. Scenes in the final column are created using the EOS Worldview website https://worldview.earthdata.nasa.gov/ from satellite products provided therein. AAOD = 0.03 is demarcated by a horizontal line in the density plots in column 3. Density plots show normalised AAOD frequencies (scale not shown).	98
2.31 Top: percentage of pixels filtered out by fire and smoke masks in 2005 (left) and 2012 (right). Bottom: percentage filtered out each day from land squares in Australia for the two years shown.	100

2.32 Top: gas fields and pipelines (2018) for Australia (http://www.ga.gov.au/scientific-topics/energy/resources/petroleum-resources/gas). Bottom: petrol Well locations over Australia (as of 2018) (http://dbforms.ga.gov.au/www/npm.well.search)	101
2.33 Forest coverage, coloured by predominant tree species.	102
2.34 Mean (top left) and standard deviation (top right) of OMNO2d daily $0.25^\circ \times 0.25^\circ$ tropospheric cloud filtered NO ₂ columns. Time series for Australia, and each region (by colour) shown in the bottom panel, with mean for that region shown on the right. The grey shaded area depicts the 25th to 75th percentiles of Australia averaged NO ₂ columns for each day in the time series, with a thicker black line showing the Australia-wide mean value.	103
2.35 Top row: 2005 OMNO2d NO ₂ column mean before (left) and after (right) applying the threshold filters as described in the text. Bottom row: time series for Australia, and each region (by colour) shown in the bottom panel, with mean for that region shown on the right. The time series before (left) and after (right) applying the anthropogenic filter are shown, the dashed and dotted horizontal lines show daily and yearly mean thresholds respectively.	105
2.36 2005 OMNO2d NO ₂ column means (top left) and distributions (top right) for Australia, and each region shown in the area map (by colour). Vertical dashed lines show the threshold for anthropogenic influence, any columns above this value are filtered out. The vertical axis is normalised so that area under the curve adds up to unity, and as such is not important except as a visual measure of the relative width between the distributions.	106
2.37 Top: OMNO2d tropospheric NO ₂ columns averaged into $2^\circ \times 2.5^\circ$ horizontal bins for Jan, 2005. Bottom: Scatter plot of NO ₂ against smearing calculations from GEOS-Chem (\hat{S}), with points above and below the smearing threshold range of 800-4600 s coloured red and blue respectively. Points are binned by NO ₂ with and without the smearing filter applied (orange and magenta respectively). Overplotted is the mean and standard deviation (error bars) within each bin. Due to the logarithmic Y scale we only show the positive direction of standard deviations for unfiltered data.	110

2.38 Top row (left): surface temperature averaged over January and February 2005. Top row (right): correlation between spatially averaged GEOS-Chem temperatures and recalculated satellite vertical columns. Second row: GEOS-Chem surface temperatures correlated against GEOS-Chem HCHO, with different colours for each grid box, and black showing the spatially averaged correlation over time. Third row: as second row, except GEOS-Chem HCHO comes from the biogenic emissions only simulation. A reduced major axis regression is used within each gridbox using daily overpass time surface temperature and HCHO. The distribution of slopes (solid) and regression correlation coefficients (dashed) for the exponential regressions is shown in the inset panels in rows 2 and 3.	112
2.39 As Figure 2.38 but for northern Australia.	113
2.40 As Figure 2.38 but for south-western Australia. TODO: Fix y axis in subplot 322	114
2.41 Surface HCHO from GEOS-Chem overpass output (midday) on the Y axis vs surface temperatures at midday (T_{GC}) and vs maximum daily temperatures from the CPC data set (T_{CPC}). Top row: Sydney grid square scatter plot and regression with one data point for each day in the summer of 2005-2006. Bottom row: as top row except averaging over several grid boxes covering south eastern Australia (SEA: 37°S to 29°S, 146°E to 153.5°W). Grid squares with pyrogenic influence detected are removed (prior to any averaging) in the right column.	115
2.42 OMI recalculated vertical columns of HCHO on the Y axis vs surface temperatures at midday (T_{GC}) and vs maximum daily temperatures from the CPC data set (T_{CPC}). Top row: Sydney grid square scatter plot and regression with one data point for each day in the summer of 2005-2006. Bottom row: as top row except averaging over several grid boxes covering south eastern Australia (SEA: 37°S to 29°S, 146°E to 153.5°W). Grid squares with pyrogenic influence detected are removed (prior to any averaging) in the right column.	116
2.43 Flow diagram showing how OMHCHO level two swath data is read, processed, and gridded in this thesis.	118
3.1 Top-down isoprene emissions estimate formation using OMHCHORP and GEOS-Chem outputs.	127
3.2 Top left: RMA slope between modelled tropospheric column HCHO and isoprene emissions (E_{GC}) using midday (13:00-14:00 LT) values over for January 2005, per grid square at $2^\circ \times 2.5^\circ$ horizontal resolution. Top right: Squared RMA correlation coefficient for regression in top left. Bottom: Sample of correlations from four grid squares. Coloured dots in top panels correspond to the colour of the regressions shown in bottom panel.	131

3.3	Row 1: monthly slope along with 95% confidence interval both before (left) and after (right) applying the smear filter for the model grid square containing Sydney over 2005-2012. Limits used in creation of the smear filter are shown with dashed lines. Row 2: regression coefficient and data-point counts for slope shown in row 1. Additionally limits for r and n used in slope utilisation (see text) are shown with dashed lines. Row 3: slope and confidence interval using the multi-year dataset for each month. Row 4: regression coefficient and data-point counts for row 3.	133
3.4	Top left: Total column HCHO over Australia using the standard tropchem GEOS-Chem simulation. Top right: As top left except over the remote Pacific region at southern mid-latitudes. Bottom left: Background Ω_{HCHO} defined using the no isoprene emissions GEOS-Chem simulation. Bottom right: Difference between the background defined using the no isoprene emission HCHO columns over Australia and using the remote Pacific HCHO columns from the standard tropchem run at matching latitudes.	134
3.5	Top row: isoprene emissions from GEOS-Chem (a priori, left) simulation and top-down (a posteriori, right) calculations averaged over the month of January, 2005. Bottom row: the absolute (left) and relative (right) differences between the two.	135
3.6	Seasonally averaged smearing (\hat{S} , see text) over 2005. Diamonds represent grid squares which have had at least 10 (pink) or 30 (red) days removed due to the smearing filter over the season. Red crosses show where the filter has removed all data.	137
3.7	Monthly area averaged HCHO lifetime (τ in hours), with IQR shaded. Solid lines show lifetime assuming yield is 0.2, and 0.4 (higher and lower lines respectively). Coloured by regions shown in Figure 3.10.	138
3.8	Row 1: α for the average January (left) and June (right) over 2005-2012. Row 2: a priori (magenta, left axis), a posteriori (cyan, left axis), and α (black, right axis) multi-year monthly averages calculated for Sydney. Row 3: Monthly averages of the same terms in Row 2.	139
3.9	Total daily isoprene emissions (in kg) is represented by the area under the sine wave.	140
3.10	Sub-regions used in subsequent figures: Northern, North Eastern, South Eastern, South Western, and Middle. Australia-wide averages will be black or grey, while averages from within the coloured rectangles will match the colour shown here.	141
3.11	Row 1: Biogenic emissions of isoprene from GEOS-Chem (a priori, E_{GC}). Row 2: Emissions calculated using the OMI top down inversion (a posteriori, E_{OMI}). Row 3: Absolute differences between the first two rows. Midday emissions are averaged for each season (DJF, MAM, JJA, SON), and colours represent averaged areas from subregions shown in Figure 3.10. Grey dashed horizontal bars are added highlighting the scale between rows.	142

- 3.12 Regional multi-year seasonal mean a priori emissions (magenta) compared to a posteriori emissions (cyan). Error bars show the regionally averaged uncertainty. Additional horizontal dashes show the uncertainty plus effects from potential HCHO biases (discussed in Section 3.4.1) from satellite underestimation (40%) and monthly clear sky overestimation (13%). 143
- 3.13 The multi-year monthly mean (lines) and IQR (shaded) of midday (13:00–14:00 LT) isoprene emissions estimates. A priori emissions are shown by the dashed lines and hatched shaded areas show the IQR. A posteriori emissions are shown using the solid lines, with IQR shown by unshaded shaded areas. Colours denote the region over which the monthly average was taken, as in Figure 3.10. 145
- 3.14 Scatter plot of a priori emissions against a posteriori using monthly averaged grid squares as regression datapoints. Data points are created using monthly averages (of midday emissions) for each grid box for each month of summer (DJF) within each region shown. Multiple years of data are used, meaning if a region has 10 grid boxes, the 8 years of data will add up to 10 boxes \times 3 months \times 8 years = 240 data points minus filtered and zero emission squares. Plots are coloured by regions matching those shown in Figure 3.10. The linear best fit regression is inset into each plot along with the line equation and regression coefficient. The normalised distribution of each population is shown at the top and right spine of each subplot, with the right spine (facing the a priori axis) using the a priori axis and scale, and the top spine using the a posteriori axis and scale. 146
- 3.15 Top row: multi-year mean a priori emissions in Tg yr^{-1} from E_{GC} (GEOS-Chem; running MEGAN) and E_{OMI} (top-down emissions) respectively. E_{OMI} uses an assumed sinusoidal daily cycle, with daylight hours prescribed for each month: see Section 3.2.10). Bottom left and right show the absolute and relative differences, respectively. 147
- 3.16 The diurnal cycle of GEOS-Chem a priori emissions (solid line) averaged by month into hourly bins over from 2005 to 2013 are shown against top-down a posteriori (dashed line) emissions. Standard deviations for the monthly average are shaded for the a priori, and shown with error bars at 13:30 LT for the a posteriori. Top down emissions shown here are based on monthly midday emissions being the peak of a sine wave which drops to zero after and before daylight hours (see Section 3.2.10). 149
- 3.17 A priori (row 1) and a posteriori (row 2) emissions anomaly from multiyear monthly mean, split by region (see Figure 3.10). 150
- 3.18 Daily mean total column HCHO amounts from GEOS-Chem with a priori (new emissions run) and a posteriori (tropchem run) a posteriori scaled isoprene emissions, along with the recalculated OMI HCHO columns. Each row shows the average over regions in Figure 3.10. 152

3.19 Total column HCHO before (left) and after (middle) scaling isoprene emissions, and their relative differences (right). Top row shows summer (DJF) averaged total columns, while bottom row shows the winter (JJA).	153
3.20 Regionally and seasonally averaged HCHO total columns from GEOS-Chem and recalculated OMI measurements side by side. Each row represents one region within Australia, while each column represents from left to right: summer, autumn, winter, spring. Standard deviations are shown with error bars.	154
3.21 Monthly averaged HCHO profile over Wollongong modelled by GEOS-Chem before (VMR) and after (VMR ^a) scaling isoprene emissions. Shaded areas represent the inter-quartile range over the month.	155
3.22 Surface ozone concentrations (ppb) per region over 2005. Concentrations are shown using the left axis, and absolute differences (tropchem run - scaled run) shown in grey using the right axis.	156
3.23 TODO: share colour bars and change to relative differences. Surface (up to ~ 150 m) ozone before (left) and after (middle) scaling isoprene emissions, and their relative differences (right). (TODO: UPDATE TO REL DIFF, UPDATE COLOUR BARS) Top row shows summer (DJF) averaged total columns, while bottom row shows the winter (JJA).	157
3.24 GEOS-Chem grid box ($2^\circ \times 2.5^\circ$) containing Wollongong FTIR, SPS, and MUMBA campaign data.	158
3.25 SPS1, SPS2, and MUMBA (left to right columns respectively) midday (13:00-14:00 local time) measurements of isoprene, HCHO, and ozone (top to bottom rows respectively). Shown in magenta and brown are the a priori and a posteriori GEOS-Chem surface outputs for the matching grid square at midday for days containing measurements.	160
3.26 Multi-year (from all days where both measurements and model data exist) monthly mean total column (Ω) HCHO from the FTIR instrument, and the colocated convolved GEOS-Chem equivalent before (Ω_{GC}) and after (Ω_{GC}^a) scaling isoprene emissions. Shaded areas show inter quartile range.	162
3.27 Median and inter-quartile range of multi-year monthly relative uncertainty in the a posteriori. Median relative uncertainty in S and Ω are added as dashed and dotted lines respectively.	165
3.28 Summer (DJF, top row) and winter (JJA, bottom row) a posteriori emissions (left column) and relative error (right column).	166
3.29 Median and inter-quartile range of monthly binned uncertainty in S	167
3.30 Mean and standard deviation (vertical error bars) of total pixel counts per region per season, before (magenta) and after (cyan) applying smearing, pyrogenic, and anthropogenic filters.	170
3.31 Median and inter-quartile range for monthly binned relative uncertainty in satellite vertical columns.	172

3.32	Top row: averaged OMI Satellite AMF for 2005, from the OMHCHO data set (left, AMF_{OMI}), recalculated using GEOS-Chem shape factors (middle, AMF_{GC}), and recalculated using GEOS-Chem shape factors and scattering weights (right, AMF_{PP}). Middle row: mean and interquartile range over 2005 for each season. Bottom row: mean and interquartile range of non-zero emissions based on the three recalculations (with matching subscripts) next to the a priori emissions from GEOS-Chem.	174
3.33	Multi-year monthly mean values for a posteriori emission estimates calculated with (solid) and without (dashed) applying filters for anthropogenic, pyrogenic, and smearing influences. The portion of pixels within each region which are filtered is shown on the right axis with a blue dotted line.	175
4.1	Ozonesonde release sites and the regions used to examine STT effect on tropospheric ozone levels.	182
4.2	Multi-year monthly median tropopause altitude (using the ozone defined tropopause) determined from ozonesondes measurements at Davis (2006-2013), Macquarie Island (2004-2013), and Melbourne (2004-2013) (solid lines). Dashed lines show the 10th to the 90th percentile of tropopause altitude for each site.	183
4.3	Multi-year mean seasonal cycle of ozone mixing ratio over Davis, Macquarie Island, and Melbourne as measured by ozonesondes. Measurements were interpolated to every 100 m and then binned monthly. Black and red solid lines show median ozone and lapse-rate defined tropopause altitudes (respectively), as defined in the text.	184
4.4	An example of the STT identification and flux estimation methods used in this work. The left panel shows an ozone profile from Melbourne on 8 January 2004 from 2 km to the tropopause (blue dashed horizontal line). The right panel shows the perturbation profile created from band-pass filtering of the mixing ratio profile. The STT occurrence threshold calculated from the 95th percentile of all perturbation profiles is shown as the orange dashed line, and the vertical extent of the event is shown with the purple dashed lines (see details in text). The ozone flux associated with the STT event is calculated using the area outlined with the orange dashed line in the left panel.	186
4.5	Seasonal cycle of STT event frequency at Davis (top), Macquarie Island (middle), and Melbourne (bottom). Events are categorised by associated meteorological conditions as described in the text, with low pressure fronts (“frontal”) in dark blue, cut-off low pressure systems (“cut-off”) in teal, and indeterminate meteorology (“misc”) in cyan. Events that may have been influenced by transported smoke plumes are shown in red (see text for details).	190
4.6	Seasonal distribution of STT events using the alternative STT proxy, obtained from consideration of the static stability at the ozone and lapse rate tropopauses, for Davis (2006-2013), Macquarie Island (2004-2013), and Melbourne (2004-2013).	191

4.7	The distribution of STT events' altitudes at Davis (top), Macquarie Island (middle), and Melbourne (bottom), determined as described in the text. Events are coloured as described in Fig. 4.5.	192
4.8	The distribution of STT events' depths, defined as the distance from the event to the tropopause, at Davis (top), Macquarie Island (middle), and Melbourne (bottom), determined as described in the text. Events are coloured as described in Fig. 4.5.	193
4.9	Comparison between observed (black) and simulated (pink, red) tropospheric ozone columns (Ω_{O_3} , in molecules cm^{-2}) from 1 January 2004 to 30 April 2013. For the model, daily output is shown in pink, while output from days with ozonesonde measurements are shown in red. For each site, the model has been sampled in the relevant grid square.	194
4.10	Observed and simulated tropospheric ozone profiles over Davis, Macquarie Island, and Melbourne, averaged seasonally. Model medians (2005-2013 average) are shown as red solid lines, with red dashed lines showing the 10th and 90th percentiles. Ozonesonde medians (over each season, for all years) are shown as black solid lines, with coloured shaded areas showing the 10th and 90th percentiles. The horizontal dashed lines show the median tropopause heights from the model (red) and the observations (black).	195
4.11	Example comparisons of ozone profiles from ozonesondes (black) and GEOS-Chem (red) from three different dates during which STT events were detected from the measurements. The dates were picked based on subjective visual analysis. The examples show the best match between model and observations for each site. GEOS-Chem and ozonesonde pressure levels are marked with red and black dashes respectively.	197
4.12	Top panel: tropospheric ozone attributed to STT events. Bottom panel: percent of total tropospheric column ozone attributed to STT events. Boxes show the inter-quartile range (IQR), with the centre line being the median, whiskers show the minimum and maximum, circles show values which lie more than 1.5 IQR from the median. Values calculated from ozonesonde measurements as described in the text.	199
4.13	(Top) Tropospheric ozone, (I)mport per event, and (P)robability of event detection per sonde launch, averaged over the region above Davis. The tropospheric ozone column Ω_{O_3} (black, left axis) is from GEOS-Chem, while the STT probability P (magenta, right axis) and impact I (teal, right axis) are from the ozonesonde measurements. The STT impact is multiplied by ten to better show the seasonality. (Bottom) Estimated contribution of STT to tropospheric ozone columns over the region, with uncertainty (shaded area) estimated as outlined in Sect. 4.7. The black line shows STT ozone flux if event lifetime is assumed to be two days, with dashed lines showing the range of flux estimation if we assumed events lasted from one day to one week.	200
4.14	As described in 4.13, for the region containing Macquarie Island.	201
4.15	As described in 4.13, for the region containing Melbourne.	202

- 5.1 Sub-regions used in subsequent figures. Australia-wide averages will
be black or grey, while results from within the coloured rectangles will
match the colours shown here. 212
- 5.2 Ozone maps before (left) and after (right) scaling isoprene emissions in
GEOS-Chem for summer. The bottom panel shows the linear regression
between the runs along with a black dashed line representing the 1-1 ratio.213

List of Tables

2.1	Detection limits for MUMBA	45
2.2	OMI quality flag values table from Kurosu and Chance (2014)	53
2.3	Species or classes from the GEOS-Chem mechanism.	62
2.4	Satellite pixels remaining after filtering by active fires, smoke, and anthropogenic masking. In parenthesis are the portion of pixels filtered. . .	95
2.5	NO_2 averages (molec $\text{cm}^{-2} \times 10^{14}$) by region before and after filtering for anthropogenic emissions using 2005 data from the OMNO2d product.	104
2.6	Smearing filters or typical slopes (S) from literature.	108
2.7	Isoprene to HCHO yields and lifetime.	109
3.1	Isoprene emissions (Tg/yr) from Australia	148
3.2	Yearly trend in surface amounts (ppbvC) before and after scaling isoprene emissions.	150
3.3	Campaign measurements compared to model output [ppb].	159
3.4	Mean total column HCHO amounts in 10^{15} molec cm^{-2}	161
3.5	Relative uncertainty estimates.	163
3.6	Uncertainties in satellite total column HCHO.	171
4.1	Number of sonde releases at each site over the period of analysis.	182
4.2	Total number of ozonesonde detected STT events, along with the number of events in each category (see text).	189
4.3	Seasonal STT ozone contribution in the regions near each site, in $\text{kg km}^{-2} \text{ month}^{-1}$. In parentheses are the relative uncertainties.	203
5.1	Isoprene emissions from MEGAN and top-down estimation in Tg a^{-1} , along with ozone tropospheric column amounts in $\text{O}_3 \text{ cm}^{-2} \times 10^{17}$	211

List of Abbreviations

ACCMIP	Atmospheric Chemistry and Climate Model Inter-comparison Project
AAOD	Aerosol Absorption Optical Depth
AMF	Air Mass Factor
AOD	Aerosol Optical Depth
BVOC	Biogenic Volatile Organic Compound
CCD	Charged Coupled Device spectrometer
CPC	Climate Prediction Center
CTM	Chemical Transport Model
DOAS	Differential Optical Absorption Spectroscopy
ECMWF	European Centre for Medium-range Weather Forecasts
EDGAR	Emission Database for Global Atmospheric Research
ERA-I	ECMWF ReAnalysis (Interim)
GC-FID	Gas Chromatographer Flame Ionisation Detector
FTIR	Fourier transform Infra-Red spectrometer
GEOS	Goddard Earth Observing System
GMAO	Global Modeling and Assimilation Office
GOME	Global Ozone Monitoring Experiment
GPH	GeoPotential Height
HEMCO	Harvard-NASA Emissions Component
IQR	Inter-Quartile Range
LAI	Leaf Area Index
LT	Local Time
OMHCHO	OMI satellite HCHO product
OMHCHORP	OMI satellite HCHO product re-processed
OMI	Ozone Monitoring Instrument
MEGAN	Model of Emissions of Gases and Aerosols from Nature
MUMBA	Measurements of Urban, Marine, and Biogenic Air
NCO	National Computing Infrastructure
NDACC	Network for the Detection of Atmospheric Composition Change
NH	Northern Hemisphere
NMVOC	Non-Methane Volatile Organic Compound
(S,P)OA	(Secondary, Primary) Organic Aerosols
OMR	Ozone Mixing Ratio
PAN	PeroxyAcetyl Nitrate
PFT	Plant Functional Type
PM	Particulate Matter
PTR-MS	Proton-Transfer-Reaction Mass spectrometer
PV	Potential Vorticity
RA	Row Anomaly

RF	Radiative Forcing
RMA	Reduced Major Axis
RMSA	Root Mean Square Error
RSC	Reference Sector Correction
RTM	Radiative Transfer Model
SAO	Smithsonian Astrophysical Observatory
SH	Southern Hemisphere
SHADOZ	Southern Hemisphere Additional OZonesonde
SPS(1,2)	Sydney Particulate Studies
STT	Stratosphere to Troposphere Transport
SZA	Solar Zenith Angle
TOA	Top Of the Atmosphere
TOMS	Total Ozone Mapping Spectrometer
VOC	Volatile Organic Compounds
UCX	Universal tropospheric-stratospheric Chemistry eXtension
UV-Vis	Ultraviolet and visible
VCC	Vertical Column Corrected
VMR	Vertical Mixing Ratio
WOUDC	World Ozone and Ultraviolet Data Centre

List of Symbols

C_x	mixing ratio or mole fraction of gas 	molecules of x per molecule of air
n_x	Number density of gas x	molecules of x per unit volume of air
Ω	Vertical column	molecules per square centimetre



Chapter 1

Introduction and Literature Review

1.1 The atmosphere

The atmosphere is made up of gases held to the earth's surface by gravity. These gases undergo transport on all scales, from barbecue smoke being blown about the garden, to smoke plumes from forest fires travelling across the world and depositing in the Antarctic snow. They take part in innumerable chemical reactions along the way, largely driven by solar input and interactions with each other. Many gases are emitted into the atmosphere by soil, trees, factories, cars, seas and oceans. They are also deposited back to the surface both directly and in rainfall.

The atmosphere is made up of nitrogen (N_2 : $\sim 78\%$), oxygen (O_2 : $\sim 21\%$), and argon (Ar : $\sim 1\%$), along with water (H_2O) and *trace gases* (those that make up less than 1% of the atmosphere). Atmospheric ~~water~~ (H_2O) content can be as high as 4% depending on local conditions. Beyond these major constituents the atmosphere has a vast number of trace gases, including carbon dioxide (CO_2 : $\sim 0.4\%$), ozone (O_3 : 0.00001% to 0.001%), and methane (CH_4 : $\sim 0.4\%$) (Brasseur and Jacob 2017, Ch. 2). Trace gases in the atmosphere can have a large impact on conditions for life on earth. They combine, break apart, and react with each other affecting all surface ecosystems upon which life depends.

One important trace gas is ozone (O_3), which affects climate, human health, and ecosystem productivity. The ozone budget (the ~~systems~~ of production, loss, and transport) is relatively uncertain over Australia. This thesis focuses on ozone in the troposphere over Australia and ~~some of the~~ Southern Ocean. It also estimates emissions of isoprene, one of the important precursors to tropospheric ozone production. This chapter provides ~~some~~ background on the structure and composition of the atmosphere and introduces ~~some~~ of the key atmospheric species examined in this thesis, as well as ~~some~~ techniques used to measure and model chemistry in the atmosphere.

1.1.1 Structure

Most of the atmosphere ($\sim 85\%$) is within 10 km of the earth's surface. This is due to gravity, which causes air pressure to decrease logarithmically with altitude. Any entity is subjected to the weight of ~~all~~ the air above it, and the ~~density~~ of the atmosphere is driven by this pressure.

The atmosphere extends above the earth's surface to the edges of space. This is split into various layers, defined by the *lapse rate*: the decrease in temperature (T) with

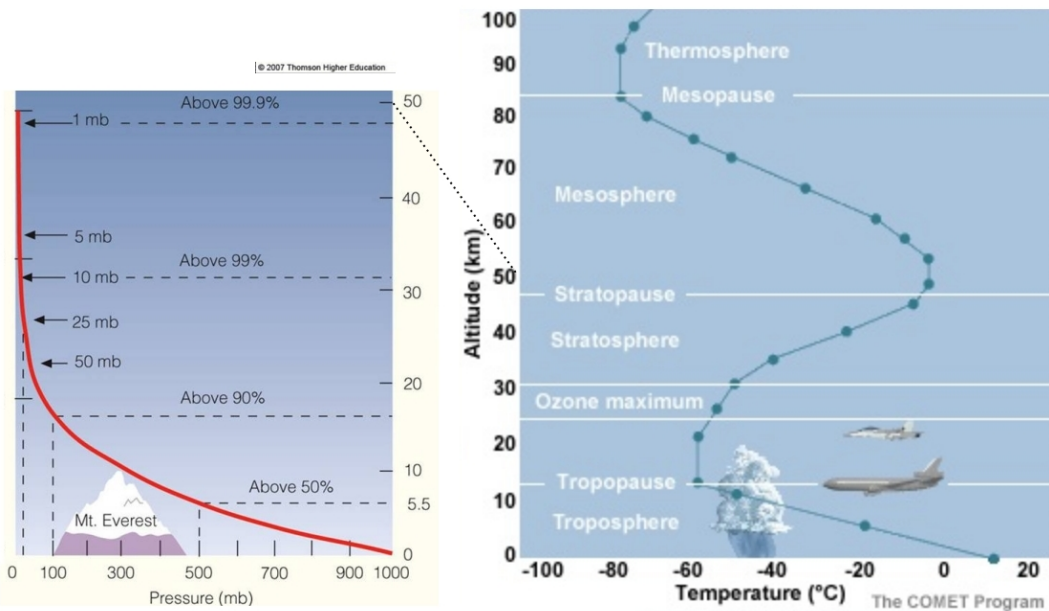


FIGURE 1.1: Pressure (red) logarithmically decreasing, shown with percentage of atmosphere below at several points. Temperature (green) changes throughout the atmosphere. Figure edited from <https://climate.ncsu.edu/edu/Structure>.

increasing altitude (z), or $\frac{-dT}{dz}$. Figure 1.1 shows the pressure and temperature profiles against altitude through the atmosphere. The first layer is the troposphere, which extends to roughly 10 km and is characterised by positive lapse rate (or decreasing temperature with altitude). At the top of the troposphere (the tropopause) the temperature stops decreasing, and then the stratosphere is defined by a negative lapse rate. This is due to ultraviolet radiation being absorbed by ozone, and leads to a very vertically stable environment.

In addition to these atmospheric layers, the troposphere can be subset into the *boundary layer* and the *free troposphere*. The *boundary layer* is the lowest layer and involves increased atmospheric mixing due to ground heating and friction effects. It generally extends from the surface up to 200 m - 1000 m, above which the ground effects have fewer direct impacts. The *free troposphere* is the remainder of the troposphere, where trace gas concentrations are more affected by transport. Transported trace gases (and particulates) can come from the stratosphere or else local to global scale winds and jet streams.

1.1.2 Composition and chemistry

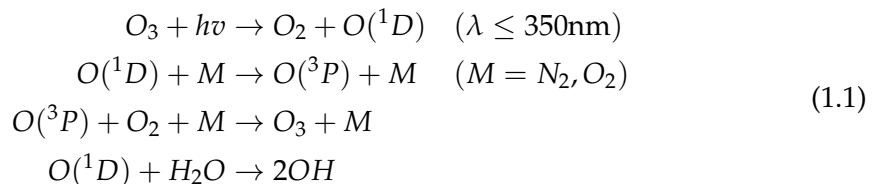
There are a myriad of trace gases in the atmosphere, emitted by plants, animals, earth, and water. These gases react with one another and over time they either deposit back onto the earth or form more stable compounds such as CO_2 . Oxidation and photolysis (the process of being broken apart by photons) are the two main processes whereby

compounds are broken down in the atmosphere. Products formed in these reactions are sometimes called children products.

OH and **HO₂** concentrations largely determine the oxidative capacity of the atmosphere. Concentration of the OH radical drives many processes in the atmosphere, especially during the day when it is produced by photolysis of ozone (Atkinson 2000). OH is a key species that reacts with nearly all the organic compounds in the troposphere, with only a few exceptions (Atkinson 2000). Over land, isoprene (C_5H_8) and monoterpenes ($C_{10}H_{16}$) account for 50% and 30% of the OH reactivity respectively (Fuentes et al. 2000).

Since radicals are involved in all oxidative chemistry in the atmosphere it is important for models to accurately represent them (e.g. Travis et al. 2016). This is difficult as they are coupled with so many other species and measurements of OH are not readily available on a global scale. In the late '90s was thought that OH radicals were formed exclusively from photolysis of O₃, HONO, HCHO, and other carbonyls (R₂C=O) (Atkinson 2000). It has been shown since that OH is recycled in various processes. Isoprene (C_5H_8) was thought to be a sink of OH until it was shown by Paulot et al. (2009b) that the radicals are recycled. This recycling process is discussed in more detail in section 1.3.3.

Ozone is an important precursor to OH, as excited oxygen atoms (O(¹D)) are created through its photolysis, which then go on to react with water to form OH, as shown in this reaction sequence (Atkinson 2000; Atkinson and Arey 2003):



Where $h\nu$ represents radiation and M is an inert molecule. This shows that some of the O(¹D) recycles back to ozone, while some form OH.

1.1.3 Radiative Forcing

One of the larger uncertainties in atmospheric modelling is how particles in the atmosphere affect radiative forcing. For some years it has been understood that aerosols have an overall cooling effect within the atmosphere. Smaller particles can match the wavelengths of visible light, interfering with incoming radiation (Kanakidou et al. 2005). Aerosol products from gas phase emissions (or the children thereof) also play an indirect and complex role in cloud properties, with a net cooling effect (Kanakidou et al. (2005), Stocker et al. (IPCC, 2013: *Climate Change 2013: The Physical Science Basis. Contribution of Working Group I to the Fifth Assessment Report of the Intergovernmental Panel on Climate Change*, Chapter 7,8)). These indirect effects are complicated, cloud creation and modification of cloud properties are particularly difficult to accurately predict. In the third IPCC report (*Intergovernmental Panel on Climate Change (IPCC): Climate Change: The Scientific Basis* 2001), the uncertainty involved from organic aerosol (OA) forcing was 3 times the estimated effect. This has since been improved, however OA and cloud formation remain as large uncertainties in more recent IPCC reports.

(Forster et al. 2007). Figure 1.2 shows the radiative forcing of various atmospheric constituents, it is clear that OA uncertainty dominates. Figure 1.3 shows the same summary updated in chapter 8 of the fifth report, where the OA uncertainty remains large.

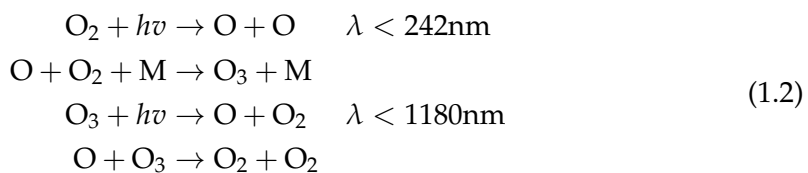
It has been known for quite a while that our understanding of volatile organic compound (VOC) emissions needs to be improved in order to better capture radiative forcing (Kanakidou et al. 2005). VOC emissions affect ozone along with several atmospheric parameters that directly and indirectly alter radiative forcing rates (e.g. Arneth et al. 2008). VOCs can lead to changes in cloud formation, as nucleation can arise from the OA formed by VOC child processes (often called secondary OA or SOA). Kanakidou et al. (2005) concluded that it is very likely that organics contribute to particle growth and formation rates, and that satellite datasets should be used to improve emissions inventories. This is even more important in Australia where VOCs are so poorly represented by contemporary modelling (Emmerson et al. 2016).

1.2 Ozone

Ozone (O_3) is an important greenhouse gas and oxidant. It is mostly located in the stratosphere and prevents much of the shorter wavelength solar radiation from reaching the earth's surface. Ozone in the troposphere is less beneficial, leading to **health issues, radiative forcing (Stevenson et al. 2013), and crop death**. Understanding and accurately portraying ozone concentrations in the troposphere is important to allow accurate predictions of future climate. This will become even more important as climate change alters the atmosphere. Projections of future climate change include changes to several atmospheric parameters such as vertical mixing rates, the ultra violet index, and ozone radiative forcing (Hegglin and Shepherd 2009).

1.2.1 Stratospheric ozone

In the stratosphere, ozone production is driven by the Chapman mechanism, as high energy radiation (with wavelengths $\lambda < 242 \text{ nm}$) photolyses the molecular oxygen (O_2) in the atmosphere (Brasseur and Jacob 2017, Chapter 3, section 2). The Chapman mechanism involves several reactions that lead to rough equilibrium of O , O_2 , O_3 and pressure, as follows:



The high energy photons ($\lambda < 242 \text{ nm}$) are present from the top of the atmosphere but are mostly removed before reaching the troposphere as their energy is used to split the O_2 molecules. The lifetime of O against loss by O_2 is less than a second in the troposphere, and produced O_3 quickly returns to O and O_2 , as low energy ($\lambda < 1180 \text{ nm}$) photons and M are abundant. The reduced light penetration towards the surface, in

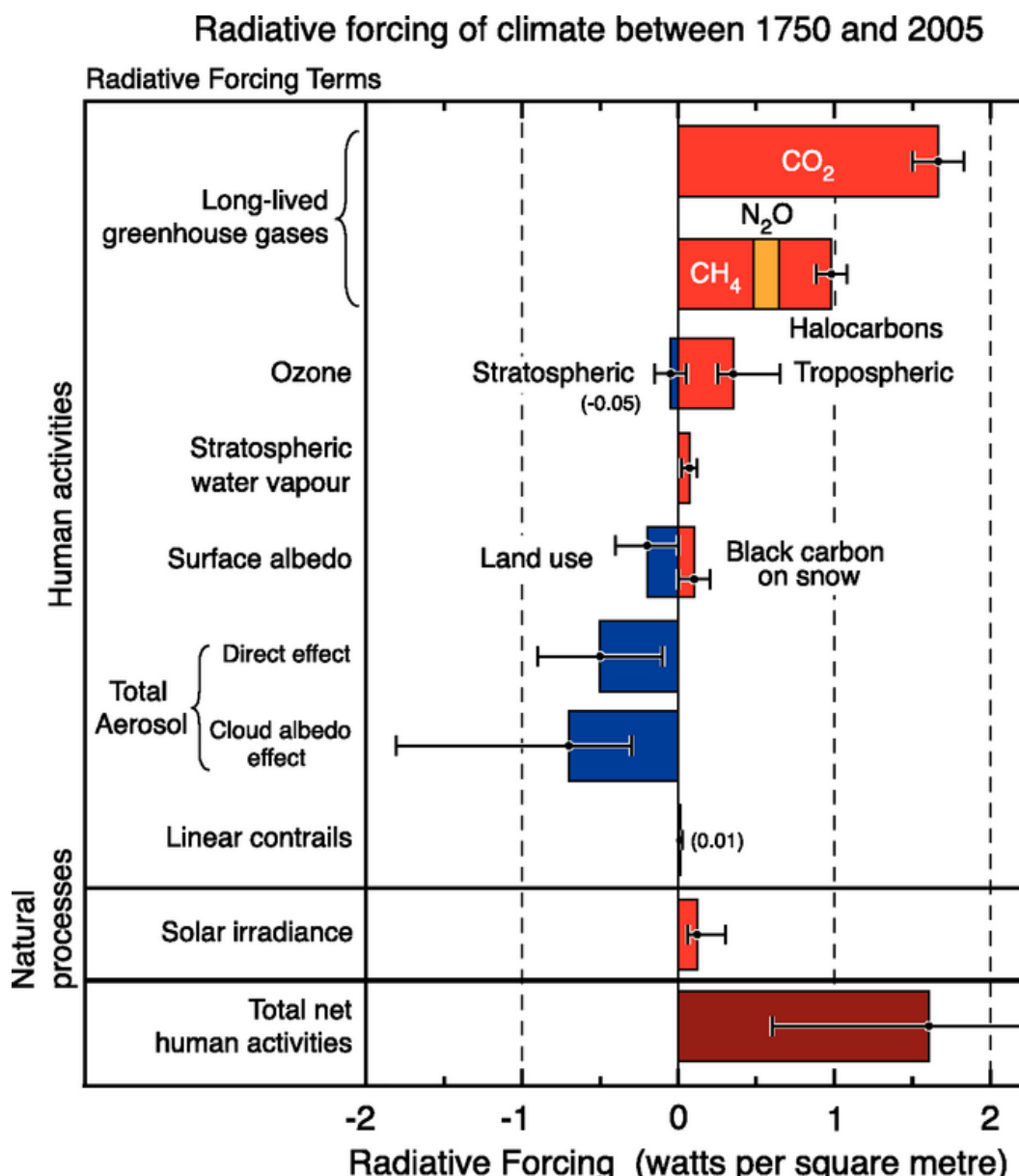


FIGURE 1.2: The overall radiative forcings and uncertainties of several atmospheric constituents This is an image taken from Forster et al. (2007), found at https://www.ipcc.ch/publications_and_data/ar4/wg1/en/faq-2-1.html.

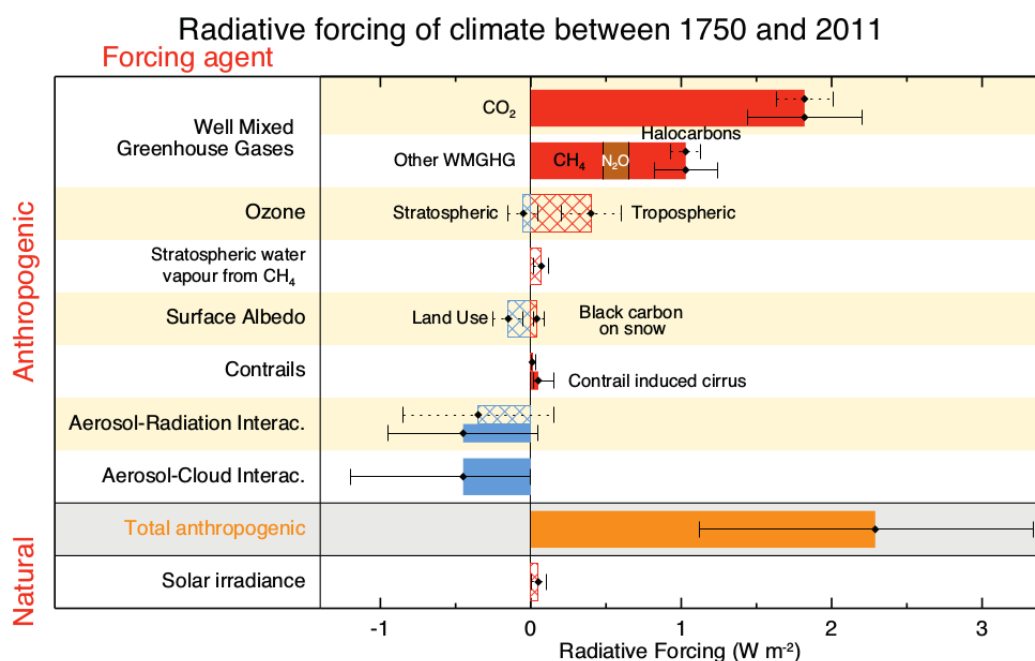


FIGURE 1.3: The overall radiative forcings and uncertainties of several atmospheric constituents This is an image taken from Stocker et al. (*IPCC, 2013: Climate Change 2013: The Physical Science Basis. Contribution of Working Group I to the Fifth Assessment Report of the Intergovernmental Panel on Climate Change*), chapter 8.

addition to the logarithmic increase in atmospheric pressure (which affects M abundance) drives the vertical profile of ozone into what is called the *ozone layer*. This is a layer of relative ozone abundance within the stratosphere. The Chapman mechanism requires radiation so only takes place during the daytime, during the night this process slows to a halt, and the ozone concentrations remain stable unless pollution intrudes (Jacob 1999, Chapter 10).



Since the Montreal Protocol on Substances that Deplete the Ozone Layer was established in August 1987, and ratified in August 1989, several satellites and many measurement stations were set up to monitor ozone in the stratosphere. However, in the southern hemisphere there are relatively few records of ozone (Huang et al. 2018). This affects our ability to accurately determine sources of ozone in the troposphere, with current southern hemisphere trends lacking full explanation (Zeng et al. 2017).



1.2.2 Tropospheric ozone

Ozone in the lower atmosphere is a serious hazard that causes health problems (Hsieh and Liao 2013), causes billions of dollars of damage to agricultural crops (Avnery et al. 2013; Yue et al. 2017), and increases the rate of climate warming (Myhre and Shindell 2013). Around 5 to 20 percent of all air pollution related deaths are due to ozone (Monks et al. 2015), which translates to roughly 800 thousand deaths per year (Lelieveld et al. 2013). In the short term, ozone concentrations of ~50-60 ppbv over eight hours or ~80 ppbv over one hour are agreed to constitute a human health hazard (Ayers and Simpson 2006; Lelieveld et al. 2009). Long term exposure causes problems with crop loss and ecosystem damage (Ashmore, Emberson, and Murray Frank 2003), and concentrations may get worse in the future (Lelieveld et al. 2009; Stevenson et al. 2013). Further tropospheric ozone enhancements are projected to drive reductions in global crop yields equivalent to losses of up to \$USD₂₀₀₀ 35 billion (equivalent to US dollars in the year 2000) per year by 2030 (Avnery et al. 2013), along with detrimental health outcomes equivalent to ~\$USD₂₀₀₀ 11.8 billion per year by 2050 (Selin et al. 2009). Recently Yue et al. (2017) showed that the net effect of near-surface ozone is an approximately 14% decrease in net primary productivity in China. They also state that in order to wind back most of this productivity decrease, drastic measures are required.

Figure 1.4, reproduced from Young et al. (2017), shows a summary of the major processes and emissions affecting tropospheric ozone. This thesis focuses on improving the highly uncertain natural emissions of volatile organic compounds (VOC) from Australia, and estimating how much ozone is transported down from the stratosphere.



Generally there are two main drivers of tropospheric ozone concentrations: transport from the stratosphere and chemical production due to emissions of precursors. Tropospheric ozone is regulated by NO and NO₂ concentrations, which form an equilibrium (Cape 2008; Young et al. 2017). At all scales, pyrogenic (fire) and anthropogenic (man-made) emissions can be important, however biogenic precursors dominate the equation globally. Smoke plumes from biomass burning can carry ozone precursors, creating higher ozone concentrations downwind of the plume's source. Emissions of precursors from large cities (primarily from traffic and power production) can impact ozone concentrations. These impacts are not always straightforward

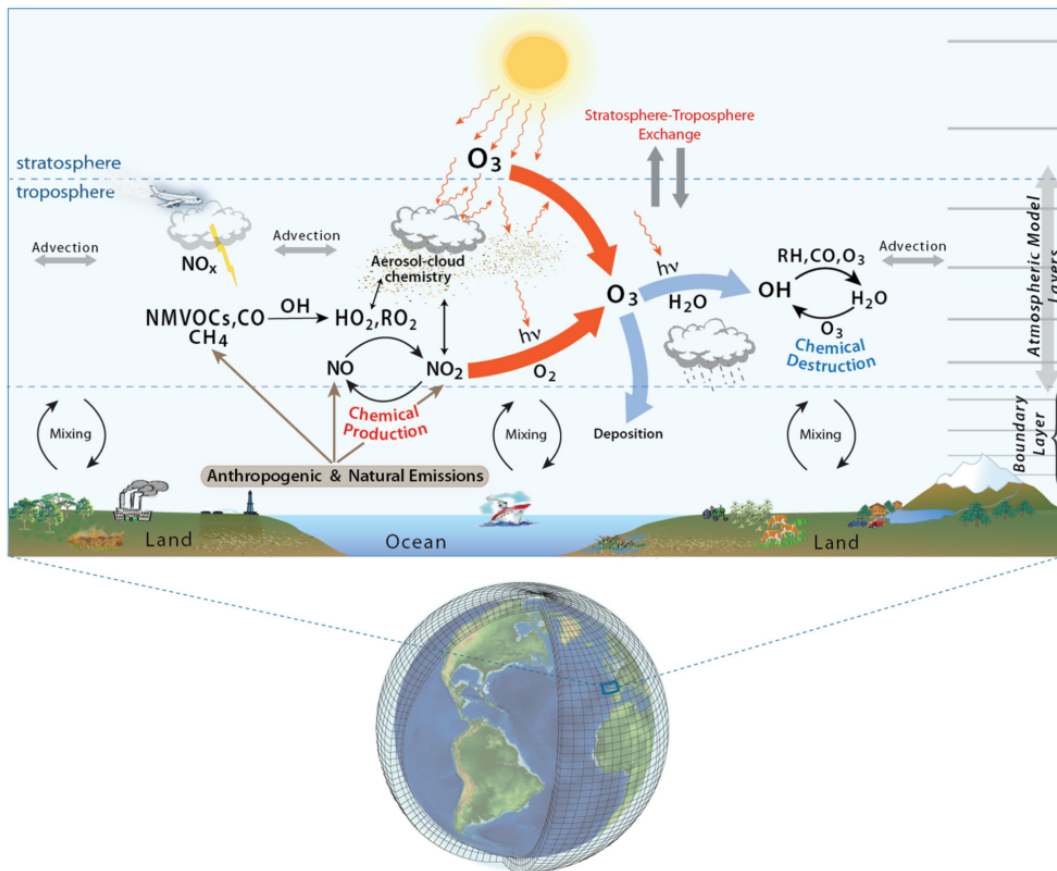


FIGURE 1.4: Tropospheric ozone processes, Figure 1 in Young et al. (2017). DOI: <https://doi.org/10.1525/elementa.265.f1>

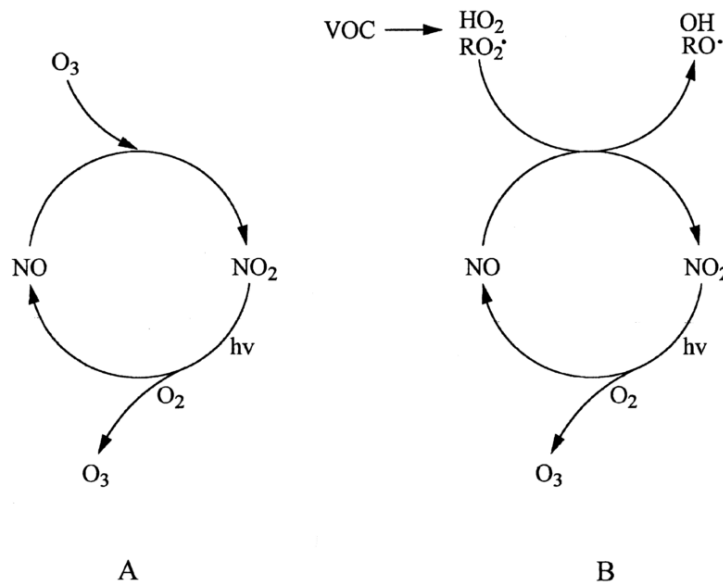
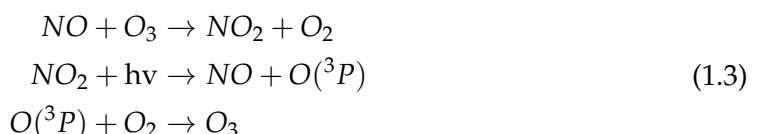


FIGURE 1.5: Figure showing the NO - NO₂ - ozone photoequilibrium cycle without and with (A, B respectively) influence from VOCs. Figure reproduced from Atkinson (2000).

due to the nonlinear relationship between ozone and its precursors. Recently, modelled ozone concentrations have been shown to be most sensitive to NO_x (\equiv NO₂ + NO) sources (such as lightning and car exhaust emissions) and isoprene emissions (Christian et al. 2018).

NO_x is an important chemical family in the atmosphere, which interacts with ozone and regulates the atmospheric oxidative capacity. NO_x or VOC emissions affect the tropospheric ozone equilibrium and can lead to enhanced ozone formation, shown in figure 1.4. NO_x compounds are short lived, with emissions from power generation and transport being the main driver of concentrations (Delmas, Serca, and Jambert 1997). NO_x is removed primarily by conversion to nitric acid (HNO₃), followed by wet or dry deposition (Ayers and Simpson 2006).

NO_x and O₃ relative concentrations during the day are regulated by the following reactions (Sillman 1999; Atkinson 2000):



VOC emissions can alter this process, essentially replacing ozone in the first stage of the above equation. The process without and with the influence of VOCs (panel A and B respectively) is summarised in figure 1.5.

1.2.3 Stratosphere to troposphere transport

Historically, ozone transported down from the stratosphere was thought to contribute 10–40 ppb to tropospheric ozone levels, making up 50% of tropospheric concentrations (Atkinson 2000; Stohl et al. 2003). The proportion was revised down to around 10% over the years as measurement and modelling campaigns improved our understanding of global scale transport, mixing, and chemistry (Guenther et al. 2006; Monks et al. 2015). Intrusions of stratospheric air into the troposphere are often called Stratosphere to Troposphere Transport (STT) events. Although most tropospheric ozone comes from production, STT enhancements of ozone are measurable and can be regionally important (eg. Dobson and Hansson 2000; Lelieveld et al. 2009; Kuang et al. 2017). Additionally, upper tropospheric ozone can be transported long distances (Cooper et al. 2004), affecting measurements far down wind where stratospheric mixing may be taking place. An analysis of the Atmospheric Chemistry and Climate Model Inter-comparison Project (ACCMIP) simulations showed STT enhances tropospheric ozone by $540 \pm 140 \text{ Tg yr}^{-1}$ (Young et al. 2013), equivalent to ~11% of the tropospheric ozone column (Monks et al. 2015).

Ozone transported to the troposphere from the stratosphere can occur through diffusion (relatively slowly) or direct mixing (as STT). STT often occurs as tongues of stratospheric air that descend into the troposphere before becoming detached. These can be due to low pressure systems and jet streams (Sprenger, Croci Maspoli, and Wernli 2003). It is possible to model this process and estimate how much ozone is being transported by STT (e.g. Young et al. 2013; Ojha et al. 2016). Model based estimates require validation against actual measurements, such as those from ozonesondes or satellites. It has been estimated that climate change will lead to increased STT through acceleration of the Brewer Dobson circulation (Hegglin and Shepherd 2009). The Brewer Dobson circulation is a large scale transport system that affects the structure and composition of the atmosphere, and meteorology, in the tropics. Hegglin and Shepherd (2009) estimated that ozone transport would increase by 23% globally by 2095 (relative to 1965), ~30 Tg yr^{-1} in the southern hemisphere and ~121 Tg yr^{-1} in the northern hemisphere.

STT mostly impacts the upper troposphere, although some areas are impacted right down to the surface. Over both oceans and land masses, STT can lead to seasonal enhancements of upper and lower tropospheric ozone concentrations (Lin et al. 2015; Liu et al. 2017a; Kuang et al. 2017). Near-surface ozone concentrations also depend on the local topography, weather systems, and trace gases emitted and transported into the region. Emissions or pollution plumes transported internationally can affect ozone concentrations, and the understanding of STT needs to be improved to allow source attribution of the causes of local ozone enhancements (Lin et al. 2015).

1.2.4 Chemical production

As discussed above, STTs source ~11% of the tropospheric column of ozone, with the remainder produced photochemically. The main processes involved are shown in figure 1.4, with reactions 1.3 regulating ozone concentrations with NO and NO_2 . A recent summary by Young et al. (2017) estimated ozone production and loss in the troposphere to be ~4900 Tg yr^{-1} , and ~4500 Tg yr^{-1} respectively. These numbers are

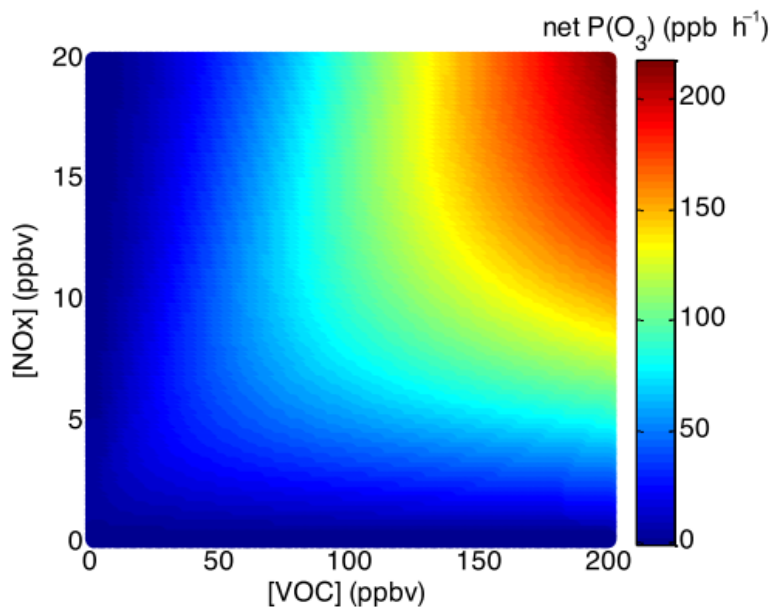


FIGURE 1.6: Ozone production rate ~~dependent~~ on NO_x and VOC concentrations (Mazzuca et al. 2016).

at the global scale, and it should be noted that meteorology and topography can play dominant roles at local to regional ~~spatial~~ scales (eg. Huang et al. 2017).

Tropospheric ozone concentrations are enhanced by ozone precursor emissions; including NO, NO_2 , CO, and VOCs such as isoprene (Atkinson 2000; Young et al. 2013; Marvin et al. 2017). Ozone predictions are uncertain and changing climate affects transport, deposition, destruction, and ~~plant-based~~ precursor emissions. All of these processes are tightly coupled and difficult to accurately model, as they depend on uncertain assumptions such as CO_2 dependency (Young et al. 2013). Even with all the work done over the prior decades there remain large uncertainties about ozone precursors in the troposphere (Mazzuca et al. 2016).

Ozone is formed in the troposphere through oxidation of VOCs (described in Section 1.3) in the presence of NO_x . Net formation or loss of O_3 is determined by interactions between VOCs, NO_x , and HO_X , and is a complicated system of positive and negative feedbacks (Atkinson 2000). Figure 1.6 shows an example of this non-linear relationship between NO_x , VOCs, and ozone production as modelled in Mazzuca et al. (2016). Essentially increasing NO_x and VOC concentrations will increase ozone production; however, increasing one or the other may or may not increase production depending on current conditions. This is a short time scale relationship and ozone production can be more or less sensitive to VOCs at different hours of the day (Mazzuca et al. 2016). It is important to correctly determine the precursors concentrations in order to estimate ozone levels and production. This non-linear relationship is examined in more detail in the following section (1.3).

 Tropospheric ozone is lost via chemical destruction and dry deposition, estimated to be $4700 \pm 700 \text{ Tg yr}^{-1}$ and $1000 \pm 200 \text{ Tg yr}^{-1}$, respectively (Stevenson et al. 2006; Young et al. 2017). The main loss channel is through photolysis and collisions, and

leads to OH production (equation 1.1).

1.3 Volatile Organic Compounds

The least well understood precursors to tropospheric ozone production belong to a subclass of organic compounds. Organic compounds are a class of chemicals whose molecules contain carbon, with the exception of a few compounds such as carbides, carbonates, and simple oxides of carbon and cyanide. Organic compounds can be categorised based on their vapour pressure, which is the tendency of a liquid or solid to vaporise. Compounds with high vapour pressures at standard temperature are classed as volatile (volatile organic compounds: VOC), and are likely to vaporise at surface pressure. Gas phase emissions  with higher vapour pressures can be oxidised into lower vapour pressure products that partition between gas and particle phase, often called semi or non-volatile. Atmospheric organic compounds are legion and differ by orders of magnitude with respect to their fundamental properties, such as volatility, reactivity, and cloud droplet formation propensity, etc.

VOCs have vapour pressure greater than 10^{-5} atm, and are mostly generated naturally by plants, which emit around 1000 Tg yr⁻¹ (Guenther et al. 1995; Glasius and Goldstein 2016). Due to their high volatility these compounds generally exist in the gas phase. Organic compounds with a lower volatility are classed as semi-volatile (SVOCs: vapour pressure between 10^{-5} and 10^{-11} atm) and are found in both gas and particle phase depending on temperature and pressure. Plants contain tens of thousands of organic compounds, with fewer than 40 having high enough volatility to be emitted (Guenther et al. 2000).

Organic compounds with even lower vapour pressure are generally found in the particle phase ~~in aerosol particulate matter~~ (Glasius and Goldstein 2016). Understanding the drivers of trends in biogenic VOC emissions (BVOCs) is required in order to estimate future carbon fluxes, changes in the water cycle, ozone production, air quality, and other climate responses (Yue, Unger, and Zheng 2015). In the last 20 years, anthropogenic emissions of VOCs have been increasing while biogenic VOC emissions have decreased, due to rapid economic growth and lower annual temperatures (Stavrakou et al. 2014; Kwon et al. 2017).

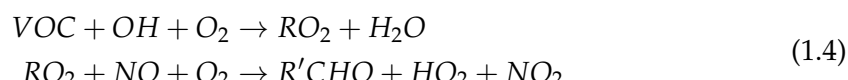
Methane (CH_4) is one of the more abundant VOCs, however it is often classified separately ~~and compared against~~ non-methane VOCs (NMVOCs). NMVOCs include alkanes, alkenes, and aromatic hydrocarbons, with isoprene (an alkene) being the most abundant (Guenther et al. 1995). Methane is relatively long lived (years) and is well mixed in the atmosphere, while other VOCs have shorter lifetimes and therefore their concentrations are more spatially variable. VOCs with short lifetimes are generally only ~~in~~ high concentrations near their emission sources.

VOCs are oxidised in the atmosphere (mainly by OH), forming HCHO, O₃, CO₂ and many other species. VOC emissions result in radical cycling, acid deposition, production of tropospheric ozone, and secondary organic aerosols (SOAs) (Atkinson 2000; Kanakidou et al. 2005). VOC emissions affect surface pollution levels, potentially enhancing particulate matter (PM) and ozone levels. A regional-model study in Europe (Aksoyoglu et al. 2017) has also shown VOCs impact secondary inorganic



aerosol concentrations. These emissions impact the climate (through radiative forcing) and can lead to lower air quality (from ozone and SOA enhancements), affecting both human health and crop yields (Forster et al. 2007; Avnery et al. 2013; Lelieveld et al. 2015).

 Ozone in rural areas is often higher than in populous cities, due to titration (removal) of ozone by NO in areas with high anthropogenic emissions (Cooper, Gilge, and Shindell 2014; Monks et al. 2015). In areas with high VOC concentrations, ozone production may be enhanced through the following reaction sequence (Sillman 1999):



with R and R' representing organic species. The reactions of VOCs with OH convert NO to NO₂, which leads to ozone formation as NO₂ production in reaction 1 of 1.3 is bypassed.

One aspect associated with VOC emissions is the production of aerosols. Aerosols are suspended particulates and liquid compounds in the atmosphere, often called particulate matter (PM). PM in the atmosphere is a major problem, causing an estimated 2-3 million deaths annually (Hoek et al. 2013; Krewski et al. 2009; Silva et al. 2013; Lelieveld et al. 2015). Fine particulate matter (PM_{2.5}) penetrates deep into the lungs and is detrimental to human health. Some PM comes from small organic aerosols (OA) that are directly emitted to the atmosphere in the particulate phase. ~~These are referred to as primary OA (POA).~~

 A substantial amount of PM is due to gaseous organic compounds transforming into what is known as secondary OA (SOA) (Kroll and Seinfeld 2008). Formation of SOA is generally due to VOC oxidation and subsequent reactions, while removal from the atmosphere is largely due to wet or dry deposition, and cloud scavenging (Kanakidou et al. 2005). ~~It can be difficult to attribute the formation of SOA, in part due to the complex relationship between NO_x, OH, O₃, and the uncertainty surrounding precursor emissions.~~ Most of the tropospheric SOA comes from biogenic precursors, ~~the evidence for this has grown over the last two decades (Guenther et al. 1995; Kanakidou et al. 2005; Guenther et al. 2012).~~ Improved concentration estimates of these precursors requires a better understanding of their emissions, which is one of the foci in this thesis.

 VOCs are removed mainly by photolysis and oxidation ~~forming alkyl radicals (R'). Additional losses are caused by wet and dry deposition, reaction with NO₃, and ozonolysis (at night time or in polluted areas) (Atkinson and Arey 2003; Brown et al. 2009).~~ The process of deposition only accounts for a small fraction of the VOC loss, ~~with the possible exception of the long lived methane compound~~ (Atkinson and Arey 2003).

1.3.1 Emissions

VOC emissions are classified as either biogenic (BVOC), anthropogenic, or pyrogenic. Global VOC ~~levels~~ are estimated to come from 85 % biogenic, 13 % anthropogenic, ~~and 3 % pyrogenic sources respectively (Kanakidou et al. 2005; Kefauver, Filella, and Peñuelas 2014).~~ Methane makes up a third of atmospheric VOCs and is relatively

ubiquitous due to its longer lifetime, non-methane VOCs (NMVOC) are often grouped together. Due to the lack of in-situ ground based measurements, estimates of VOC emissions are uncertain, with large scale extrapolation required (Millet et al. 2006). The ocean also plays a role in VOC emissions, with the Oceanic Niño Index showing positive VOC emission anomalies associated with neighbouring countries (Stavrakou et al. 2014).

The main non-methane BVOC emissions are isoprene (44%) and monoterpenes (11%) (Guenther et al. 2000; Kefauver, Filella, and Peñuelas 2014). There are ten times the mass of NMVOCs from natural sources as there are from anthropogenic sources (Guenther et al. 2006; Kanakidou et al. 2005; Millet et al. 2006). Major emitters are broadleafs (notably Eucalyptus), and shrubs (Guenther et al. 2006; Arneth et al. 2008; Niinemets et al. 2010; Monks et al. 2015). NMVOC emissions are a byproduct of photosynthesis, and also a response to various environmental factors, including temperature, atmospheric CO₂, soil moisture, drought stress, etc. Land use changes can drastically affect isoprene sources, for instance in the tropics where large scale deforestation has converted forest into crop lands (Kanakidou et al. 2005). In this thesis I focus on emissions of isoprene in Australia.

Globally around 710 - 1150 Tg C yr⁻¹ of BVOCs are emitted (Guenther et al. 1995, Lathière et al. 2006; Guenther et al. 2012; Messina et al. 2016). 90% of these emissions come from plants and trees, with the most dominant species being isoprene (C₅H₈) (~ 50%), and ~ 30% from monoterpenes (C₁₀H₁₆), methanol (CH₃OH), ethanol (C₂H₆O), acetaldehyde (CH₃CHO), acetone ((CH₃)₂CO), ethene (C₂H₄) and propene (C₃H₆) (Guenther et al. 2012). Many of these estimates come from MEGAN, a bottom-up biogenic emissions model that is highly sensitive to several parameters including soil moisture and plant functional type.

MEGAN “is a modelling framework for estimating fluxes of biogenic compounds between terrestrial ecosystems and the atmosphere to account for the major known processes controlling biogenic emissions” (Guenther et al. 2012).

MEGAN allows parameterisation of various BVOC emissions, with descriptions given in Guenther et al. (2012). One recent analysis has estimated that isoprene makes up 70% (532 Tg C yr⁻¹ of 760 Tg C yr⁻¹) of the BVOC emissions (Sindelarova et al. 2014). MEGAN emissions estimates are termed bottom-up, as opposed to top-down, which are derived from satellite measurements of the products of various VOCs. For example, GOME satellite HCHO and a Bayesian inversion technique have been used to estimate isoprene emissions of ~566 Tg C yr⁻¹ globally (Shim et al. 2005).

1.3.2 Isoprene

Isoprene (2-methylbuta-1,3-diene) is a VOC with the chemical formula C₅H₈. It is of major importance to the atmosphere, as it is involved in various processes that alter the oxidative capacity of the atmosphere. Isoprene affects NO_x and HO_x cycling, see for example formulae 1.1, 1.3. In the presence of NO_x, isoprene forms tropospheric ozone and SOAs (Wagner 2002; Millet et al. 2006). It has a short lifetime during the day, roughly an hour due to OH oxidation (Atkinson and Arey 2003)).

Measurements of isoprene are often uncertain, as the compound is reactive and short lived. Chamber experiments are used to determine how isoprene behaves once it is emitted into the atmosphere; however, laboratory derived reaction rates may be unsuitable when modelling the natural atmosphere, which is often very different (Kanakidou et al. 2005; Nguyen et al. 2014). Improving chamber study methods could improve understanding of ambient atmospheric oxidation mechanisms of isoprene (and other organic hydrocarbons), which could reduce some of the high uncertainties involved with VOC chemistry (Nguyen et al. 2014). Structural uncertainties (differences between different measurement techniques, see Section 1.4.2) in measurements also occur, which increases the difficulty of assessing isoprene data-sets.

Guenther et al. (1995), and subsequent updates (Guenther et al. 2000; Guenther et al. 2006; Guenther et al. 2012), have been used ubiquitously by the atmospheric community as a global estimate of isoprene emissions, at roughly $500\text{--}600 \text{ Tg yr}^{-1}$, emitted mostly during the day. Recently an estimate of global isoprene emissions, of around 465 Tg C yr^{-1} ($\sim 527 \text{ Tg yr}^{-1}$ isoprene), has been made using a completely different model (Messina et al. 2016). The global emission factors used to derive both these estimates are based on modelling emissions from different plant species (phenotypes), and relatively few Australian species are used when forming these estimates. This leads to increased uncertainty for Australian emissions estimates. Due to the highly reactive nature of isoprene, modelling is sensitive to uncertainties, for example the diurnal pattern of isoprene emissions affects modelled ground level ozone (Hewitt et al. 2011; Fan and Zhang 2004).

The global uncertainty of isoprene emission was estimated to be a factor of 2 to 5 ($250\text{--}750 \text{ Tg yr}^{-1}$) (Kanakidou et al. 2005). Improvements over the years have been incremental, and generally localised to regions of particular interest for air quality such as China and the USA (Guenther et al. 2012; Jiang et al. 2018). The lack of accuracy in BVOC emissions measurements (in general) prevents accurate determinations of the sources and distribution of pollutants including ozone and organic aerosols.

1.3.3 Isoprene chemistry

Isoprene is emitted and enters the atmosphere in the gas phase, where it reacts quickly with OH and other radicals. One common compound that is produced by these reactions is HCHO, which can be measured from satellites and is often used to estimate how much isoprene is being emitted. Isoprene (and other alkenes, organic compounds with double bonded carbon) reacts with OH, ozone, or NO_3 , leading to organic peroxy radicals (ROO'). These go on to form many products and lead to (amongst other things) aerosol, formaldehyde, and ozone formation, depending on sunlight and NO_x concentrations (Atkinson 2000). Reactions with NO can lead to ozone production within environments rich in isoprene or other NMVOCs (Patchen et al. 2007; Atkinson and Arey 2003).

Figure 1.7 shows the first stages of oxidation of isoprene by OH. Isoprene reactions are important to understand due to their impacts on air quality, ozone, and physical properties in the lower troposphere. The primary first step for atmospheric isoprene is photooxidation, reacting with OH to form isoprene hydroxyperoxy radicals (ISOPOO (a subset of ROO')) (Patchen et al. 2007; Wolfe et al. 2016; Marvin et al. 2017). This is largely split into two types of ISOPOO, based on which carbon the OH adducts to (see

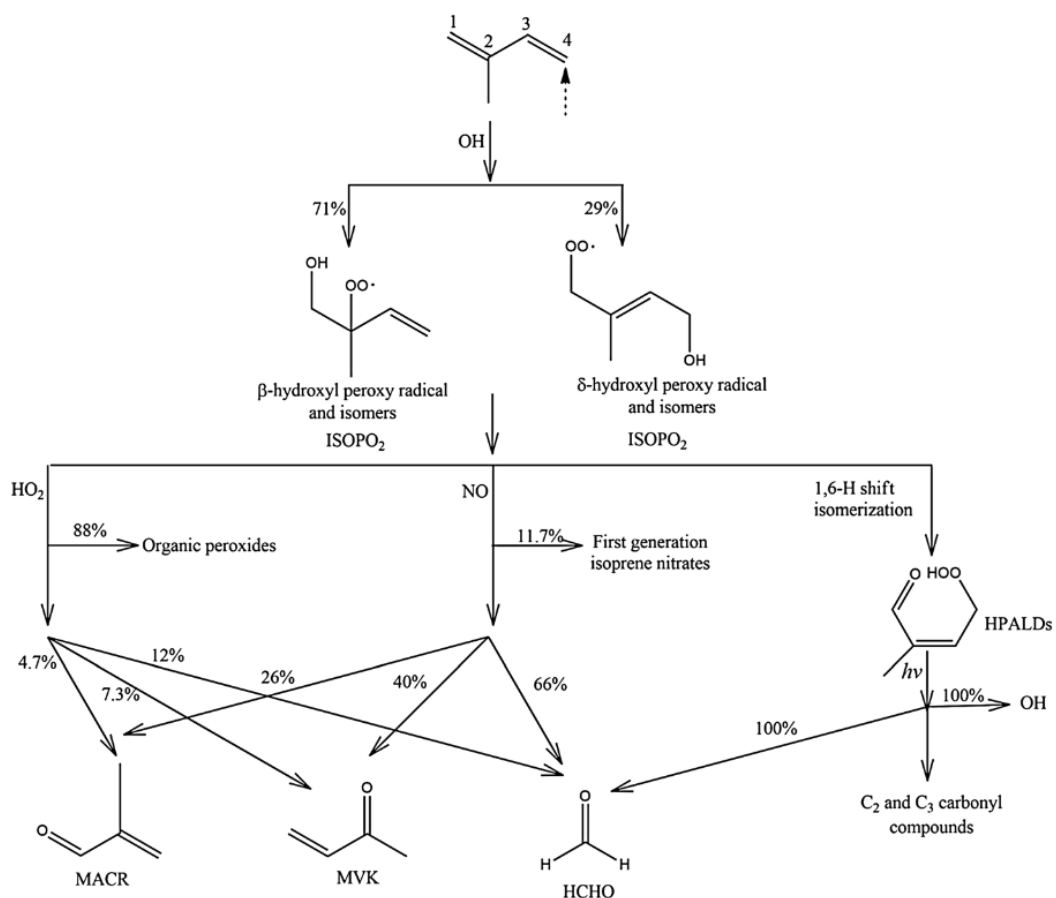


FIGURE 1.7: Isoprene products following oxidation by OH, figure from Mao et al. (2013)

figure 1.7).



The many children processes and products that begin with isoprene oxidation are often called the isoprene (photochemical) cascade (eg. Crounse et al. 2012; Paulot, Henze, and Wennberg 2012; Wolfe et al. 2016).

1.3.3.1 Oxidation

The primary sink for isoprene is oxidation by OH. First isoprene has its double bond replaced by OH, as summarised by the equation: $R-\text{CH}=\text{CH}-R' + \text{OH} \rightarrow R-\text{CH}(\text{OH})\text{CH}-R'$, where R and R' represent hydrocarbons (Patchen et al. 2007). Ozonolysis and photolysis are lesser oxidation pathways for volatile alkenes, involving the splitting of carbon chains by ozone molecules or photons respectively:



(Nguyen et al. 2016; Wolfe et al. 2016). Ozonolysis also leads to HCHO, with yields depending on subsequent reactions.

After oxidation by OH, the adducted OH then reacts with O_2 to produce ISOPOO, which can be any of six different isomers (Patchen et al. 2007). ISOPOO reacts with HO_2 or NO, producing stable products (often called oxidised VOCs or OVOCS). This pathway also produces HCHO (with varying yields):



During the day HCHO has a lifetime of 1-2 hrs, while ROO lasts ~ 100 s, making reaction 1.5 a rate limiting factor in HCHO production (Wolfe et al. 2016). ISOPOO also can isomerise and produce hydroperoxy-methyl-buteneals (HPALDS) (see figure 1.7), which also leads to HCHO. At higher NO mixing ratios (at least a few hundred pptv), ROO react mostly with NO. At low NO (less than 50 pptv), ROO is more likely to either isomerise, react with HO_2 , or react with another ROO.

There is uncertainty about which pathways are most important following ISOPOO production, affecting predictions by atmospheric models (Nguyen et al. 2014). This limits understanding of the relative importance of some chemical processes, such as auto-oxidation (of ISOPOO and other ROO) (Crounse et al. 2013). The reaction pathways depend on local concentrations of NO_x : the high and low NO_x pathways are dominated by NO and HO_2 reactions respectively. HO_2 reactions predominantly produce hydroxyhydroperoxides (ISOPOOH), while NO reactions produce isoprene nitrates (ISOPN) (Crounse et al. 2006). If measured, first generation ISOPN and ISOPOOH products can be used to determine the portion of isoprene oxidation following each pathway (eg. Yu et al. 2016). Globally around one third of ISOPOO react with HO_2 , and two thirds react with NO (Paulot et al. 2009b). Most of these reaction pathways produce HCHO, however this along with methyl vinyl ketone (MVK), and methacrolein (MACR) are formed at different yields between the two pathways (Marais et al. 2012; Liu et al. 2016b; Wolfe et al. 2016).

1.3.3.2 High NO_x pathway

In the presence of NO_x, ISOPOO reacts with NO and forms ISOPN, which affect levels of both HO_x (H, OH, peroxy radicals) and NO_x. ISOPN generally act as a sink of HO_x, and can be a sink or reservoir for NO_x (Mao et al. 2013). A portion of the ISOPN are recycled back to NO_x, serving as a reservoir of nitrogen and allow its transport to the boundary layer of remote regions (Patchen et al. 2007; Paulot et al. 2009a; Yu et al. 2016). The nitrates can also build up in the winter, when removal processes are not as dominant (Lelieveld et al. 2009). Reactions of OH with NO₂ are the main radical sink in high-NO_x systems (Wolfe et al. 2012).

Under high NO_x conditions there is a higher and faster yield of HCHO, with most of the ultimate HCHO production occurring within one day (Palmer et al. 2006). First generation ISOPN produce MVK($\sim 40\%$), MACR($\sim 26\%$), and HCHO($\sim 60\%$) at higher yields than is produced by ISOPOOH (Liu et al. 2013; Mao et al. 2013). The MVK and MACR products form additional HCHO within a few hours due to oxidation by OH (Palmer et al. 2006).

1.3.3.3 Low NO_x pathway

In low NO_x environments, ISOPOOH is formed in yields $> 70\%$, while MACR, MVK, and HCHO are formed at $\sim 5\%$, $\sim 7\%$, and $\sim 12\%$ respectively (Paulot et al. 2009b; Mao et al. 2013). This ISOPOOH mostly reacts with OH to form IEPOX while regenerating OH (Mao et al. 2013). This pathway has lower and slower ultimate yields of HCHO from isoprene emissions when compared to the high-NO_x pathway (Palmer et al. 2006).

Isoprene oxidation and subsequent reactions are less well understood when lower concentrations of NO are present in the atmosphere. It was thought that in low NO environments, like those far from anthropogenic pollution and fires, oxidation of isoprene would create ISOPOOH and reduce local concentrations of OH and HO₂ (Guenther et al. 2000; Paulot et al. 2009b). However this reduction was not seen in measurements and HO_x levels have been shown to be largely unaffected by isoprene concentrations (Paulot et al. 2009b). HO_x is recycled through dihydroxyperoxides (IEPOX) formed from ISOPOOH oxidation, and some HO_x is produced in the formation of MACR and MVK (Paulot et al. 2009b). Paulot et al. (2009b) estimated that $95 \pm 45 \text{ Tg yr}^{-1}$ of IEPOX was being created in the atmosphere, which (at the time) was not modelled by CTMs. Peeters and Muller (2010) suggested that the work of Paulot et al. (2009b) only partially bridges the gap between clean air OH concentration measurements and models. They suggested four new mechanisms for OH recycling in these pristine conditions. These can be summarised as OH regenerating reactions that occur during photolysis of HPALDs, and resulting photolabile peroxy-acid-aldehydes (PACALDs). These reactions are highly non-linear and subject to large uncertainty, however they were shown to improve modeled HO_x concentrations against several campaigns. OH regeneration and HO₂ production at near unity yields following isoprene oxidation initiated by OH has been measured independently (Peeters and Muller 2010; Crounse et al. 2012).

Uncertainties and bias from measurements have made it more difficult to understand what happens in low NO_x conditions, and many observations of OH were still

~~quite~~ under-predicted in models (Mao et al. 2012). Due to OVOC interference, measurements in low NO_x environments can lead to massively overestimated MVK and MACR yields (Nguyen et al. 2014). Nguyen et al. (2014) show preliminary estimates of low-NO yields of MVK and MACR to be 6±3% and 4±2% respectively, consistent with Liu et al. (2013), but only when cold-trapping methods are employed. Many instruments have been shown to generate OH internally, creating anomalous VOC readings due to within-instrument oxidation (Mao et al. 2012).

Improved understanding of both the chemistry and instrument sensitivities has helped closed the gap between model predictions and detected concentrations of VOCs and OH (Mao et al. 2012). But even with the recent boom in analysis, uncertainties remain in isoprene oxidation mechanisms. Examples (taken from Nguyen et al. (2014)) include:

- isoprene nitrate yields, which range from 4-15% (Paulot et al. 2009a) 
- 90% disagreements in MACR and MVK yields (Liu et al. 2013)
- various possible sources for SOA (Chan et al. 2010; Surratt et al. 2010; Lin et al. 2013) 
- unknown HPALD fates and incomplete O₂ incorporation (Peeters, Nguyen, and Vereecken 2009; Crounse et al. 2013) 
- under-characterised RO₂ lifetime impacts (Wolfe et al. 2012).

1.3.3.4 Night time processes

At night when OH concentrations have dropped, isoprene can remain in the atmosphere. Typically less than half of this night time isoprene is removed through ozonolysis (Atkinson and Arey 2003). A build up of NO₃ radicals can be seen at night, when photolysis is not removing them (Atkinson 2000; Brown et al. 2009). This build up is enhanced in polluted (high NO_x) areas. NO₃ are largely formed through ozone reactions, as in equation 1.3. In these conditions isoprene is consumed by nitrate radicals (NO₃) that join to one of the double bonds, producing organic nitrates (RONO₂) in high yield (65% to 85%) (Mao et al. 2013).  

In areas with high NO_x levels, greater than 20% of the isoprene emitted late in the day ends up being oxidised by the NO₃ radical overnight (Brown et al. 2009). At night isoprene affects both NO_x concentrations and ozone levels, and can form harmful organic nitrates and SOA (Brown et al. 2009; Mao et al. 2013). These nitrates go on to produce further SOAs, largely due to NO₃ reacting with first generation isoprene oxidation products (Rollins et al. 2009). The night-time concentrations of OH and ozone also have a complex effect on NO_x removal in high latitude winters, when photolysis and NO reactions are reduced (Ayers and Simpson 2006).

1.4 Formaldehyde

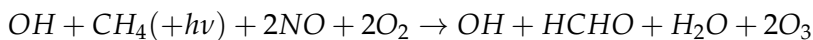
Formaldehyde (HCHO), aka methanal, methyl aldehyde, or methylene oxide, is of the aldehyde family. HCHO is an OVOC that is toxic, allergenic, and a potential carcinogen. Generally, HCHO is not dangerous at low background atmospheric levels.

Globally, HCHO production is due to the oxidation of methane; however, over continental regions, HCHO enhancement above the background level is largely due to isoprene emissions. Given a modelled yield of HCHO from isoprene, it is possible to work backwards from measured HCHO concentrations to determine the isoprene emissions. HCHO production also depends on NO_x concentrations, which affect the yield from isoprene oxidation. HCHO yield is higher in the high-NO_x pathway (compared to the low-NO_x pathway) from isoprene reactions (Marais et al. 2012). HCHO measurements are often used as a check on how well isoprene reactions are simulated, as HCHO levels depend on initial VOCs and oxidants (which can be prescribed) (Marvin et al. 2017).

Isoprene reaction chains are diverse, with many branches forming HCHO. HCHO production yields are often classed into two categories: first generation HCHO yield and total (or molar) yield. First generation yield refers to the amount of HCHO produced per unit isoprene consumed by initial oxidation. Total yield refers to the time-dependent yield of HCHO over multiple oxidation stages (Wolfe et al. 2016). In this work (Section 3.2.4) a function of the yield (the slope $S = Y_{isop}/k_{HCHO}$) is calculated to link satellite measured HCHO to isoprene emissions.

1.4.1 Sources and sinks

Background levels of HCHO in the atmosphere are driven by the oxidation of methane (CH₄) by the hydroxyl radical (OH), which produces $\sim 970 \text{ Tg yr}^{-1}$ (Fortems-Cheiney et al. 2012). Atkinson (2000) summarised the background formation of HCHO with the following reaction:



This shows that photolysis and oxidation of methane forms HCHO and ozone in a process that regenerates the OH radicals. CH₄ concentrations are relatively well constrained in models, with the ACCMIP comparison showing only $\sim 3\%$ inter-quartile range (Young et al. 2013). There is a complex relationship between VOCs, HO_x, and NO_x: with higher levels of NO_x increasing the rate at which VOCs are converted into HCHO (Wolfe et al. 2016).

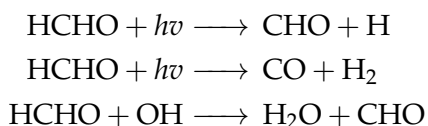
Within the continental boundary layer (CBL) HCHO is enhanced above background HCHO levels, due to NMVOC emissions reacting with OH radicals in the presence of NO_x (Wagner 2002; Millet et al. 2006; Kefauver, Filella, and Peñuelas 2014). The total contribution from NMVOC oxidation is $\sim 358 \text{ Tg yr}^{-1}$ (Fortems-Cheiney et al. 2012). Enhancements to regional and continental HCHO are largely driven by emissions of one particular NMVOC, isoprene (Guenther et al. 1995; Palmer et al. 2003; Shim et al. 2005; Kefauver, Filella, and Peñuelas 2014). This is true except near fires or anthropogenic sources of HCHO and precursors (Guenther et al. 1995; Kefauver, Filella, and Peñuelas 2014; Wolfe et al. 2016). Biomass burning (BB) can be a source of HCHO, and various other pollutants, precursors, and aerosols (Guenther et al. 1995; Andreae 2001). Additionally, HCHO is emitted into the atmosphere directly through fossil fuel combustion, natural gas flaring, ethanol refining, and agricultural activity (Wolfe et al. 2016).

Other terpenoids (monoterpenes, sesquiterpenes, etc.) can also produce HCHO, although generally to a lesser extent than isoprene, methane and biomass burning (Guenther et al. 2012). Many of the HCHO yields from terpenoids are estimated through chamber studies that examine molecular mass and charge after mixing the compound of choice into a known volume of air (eg. Nguyen et al. 2014). These conditions generally do not match those of the real world, where ambient air will have a cocktail of these compounds and other reactants. One issue with chamber studies is inaccurate reproduction of ambient outside air, which limits the scope to which the studies may be applied (Nguyen et al. 2014).

Anthropogenic sources of HCHO are largely negligible; however, their signals can be seen in very large cities or when using oversampling techniques (Millet et al. 2008; Zhu et al. 2014). If the population centres and industrial districts are large enough they can emit huge amounts of VOCs into the atmosphere (Fu et al. 2007), leading to increased surface ozone levels (Zhu et al. 2014). In Australia this is not yet a major issue, however anthropogenic sources of pollution can be detected (see section 2.7.2).

In the past, HCHO levels were underestimated by models, often with large discrepancies, due to the poor understanding of methyl peroxy radical (CH_3OO) chemistry (Wagner 2002). Nowadays HCHO concentrations are better understood, however precursor emissions are one of the main unknowns (eg. Emmerson et al. 2016; Marvin et al. 2017). The primary source of discrepancy between modelled HCHO concentrations is due to second and later generational isoprene oxidation chemistry (Marvin et al. 2017).

HCHO has two major sinks totalling $\sim 1210 \text{ Tg yr}^{-1}$, reactions with OH (oxidation), and photolysis (Levy 1972; Crutzen, Lawrence, and Poschl 1999; Wagner 2002; Fortems-Cheiney et al. 2012; Kefauver, Filella, and Peñuelas 2014). The main other sinks are wet and dry deposition, although these are not as significant ($\sim 32 \text{ Tg yr}^{-1}$) (Atkinson 2000; Fortems-Cheiney et al. 2012). Oxidation and photolysis reactions begin as follows (Ayers et al. 1997):



These reactions lead to a daytime lifetime of a few hours (Atkinson 2000; Millet et al. 2006). Both these loss processes (photolysis, oxidation) form CO, and lead to production of hydroperoxyl radicals (HO_2). These products have global significance to radiative forcing and oxidative capacity (Franco et al. 2015).

1.4.2 Measurement techniques

There are a few ways to measure HCHO; data used in this thesis has been created using two different techniques: Fourier Transform Infra-Red (FTIR) Spectrometry and Differential Optical Absorption Spectroscopy (DOAS). FTIR examines the Fourier transform of a measured spectrum in order to quantify species which interfere with the

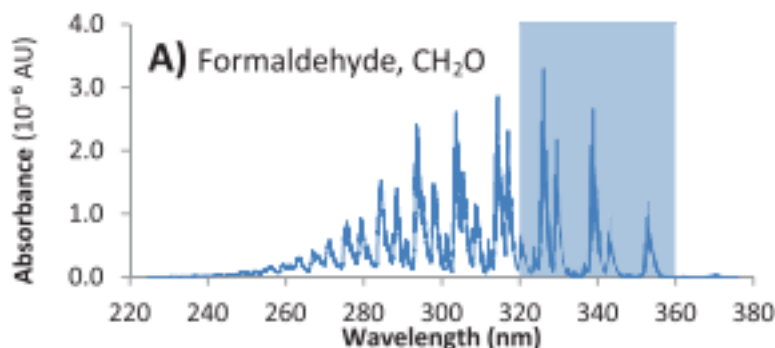


FIGURE 1.8: HCHO spectrum, with a typical band of wavelengths used for DOAS path measurements. This is a portion of an image from Davenport et al. (2015).

spectrum in the infra-red region. DOAS methods are based on light interference and absorption through air masses.

The DOAS technique takes advantage of the optically thin nature of HCHO in order to linearise the radiance differential through air masses with and without HCHO, using the Beer-Lambert intensity law. This method is used globally both from ground-based and space-based instruments for HCHO detection (Guenther et al. 1995; Gonzalez Abad et al. 2015; Davenport et al. 2015). As a trace gas HCHO interferes with light over a few wavelength bands, which allows instruments to detect concentrations between a known light source and a detector. Figure 1.8 shows the interference spectrum of HCHO along with a typical band used to examine interference in the DOAS technique. FTIR and DOAS measurements have a range of uncertainties, including systematic and random measurement errors and uncertain a priori shape factors and water profiles (e.g. Franco et al. 2015). One difficulty is that this interference is relatively small (HCHO is optically thin) and other compounds absorb light at similar wavelengths (Davenport et al. 2015).

Other types of measurement involve directly measuring the air, and determining chemical compounds through their physical properties such as by mass spectrometry analysis of mass to charge ratios (m/z) of ionised air masses. Two examples of this include proton transfer reaction mass spectrometers (PTR-MS), and gas chromatography mass spectrometers (GC-MS). These instruments can be also used to determine the gas phase evolution of other isoprene and monoterpene products (eg. Lee et al. 2006; Nguyen et al. 2014; Wolfe et al. 2016; Lerner et al. 2017). Other measurement techniques include chromatographic and fluorimetric methods. These differ widely from both each other and the spectroscopic methods (Hak et al. 2005). Reasonable agreements between different instruments and techniques can be achieved, although titration and calibration differences can lead to large ($\sim 30\%$) discrepancies (e.g. Hak et al. 2005). These differences and non-uniformities between measurements (even among identical instruments) are part of the reason HCHO does not have a consistent network for global measurements like those for greenhouse gases or ozone (Fortems-Cheiney et al. 2012).

1.4.2.1 Satellite measurements

Satellites remotely sense atmospheric HCHO through irradiance measurements of solar light that has reflected off the earth's surface. These irradiances are affected by gases that exist along the reflected path of light between the detector, earth, and sun. The irradiance is then used to estimate how much of a particular gas exists along this path, which gives us an estimate called the slant column (SC). The retrieved SC of a particular gas (species) can be transformed into a vertical column (VC) by scaling the path length in conjunction with accounting for the light scattering properties of the trace gas. The scaling coefficient created to transform from SC to VC is called the Air Mass Factor (AMF).

Several satellites provide long term trace gas observations with near complete global coverage. Some of these are listed here:

- The ERS-2 launched in April 1995, housing the GOME ultraviolet and visible (UV-Vis) spectrometer
- The AURA launched in July 2004, housing the OMI UV-Vis spectrometer
- The MetOp-A and B launched in October 2006 and September 2012 respectively, both housing a GOME-2 UV-Vis spectrometer.

These satellites are on Low Earth Orbit (LEO) trajectories and overpass any area up to once per day. Satellites use DOAS techniques with radiative transfer calculations on solar radiation absorption spectra to measure column HCHO. An example of a spectrum retrieved from the GOME-2 instrument is given in figure 1.9.

Satellite based chemical concentrations often require both remote and in situ measurements combined with modelled data for validation (Marais et al. 2014). There is less information available from satellite measurements at higher latitudes due to increased error in measurements over the more slanted column paths (De Smedt et al. 2015). Validation is important due to the various uncertainties in the satellite remote sensing process. This can be done using air craft data such as from the SEAC⁴RS HCHO measurements over the southeastern US to provide model validation (e.g. Zhu et al. 2016). Satellites use an assumed shape factor to improve the vertical column estimate, however this can lead to a bias between satellite data and other measurements (Zhu et al. 2016). Different satellites, instruments, or techniques that measure HCHO (or any trace gas) can give different results due to differing a priori assumptions or applied calculations (Lorente et al. 2017). The concept of differences that arise between datasets based on measurement techniques or underlying instrument biases is called structural uncertainty.

In conjunction with atmospheric chemistry and radiative models, satellite measurements quantify the abundance of HCHO in the atmosphere. Isoprene is hard to measure directly due to its short lifetime and weak spectral absorption, instead HCHO is often used as a proxy (Millet et al. 2006; Fu et al. 2007; Dufour et al. 2008; Marais et al. 2012; Bauwens et al. 2013; Kefauver, Filella, and Peñuelas 2014; Bauwens et al. 2016; Surl, Palmer, and Abad 2018). This leads to a method of isoprene emissions estimation termed top-down (as opposed to bottom-up estimates). The existence of satellite data covering remote areas provides an opportunity to improve VOC emissions estimates leading to more robust models of global climate and chemistry. Satellite data

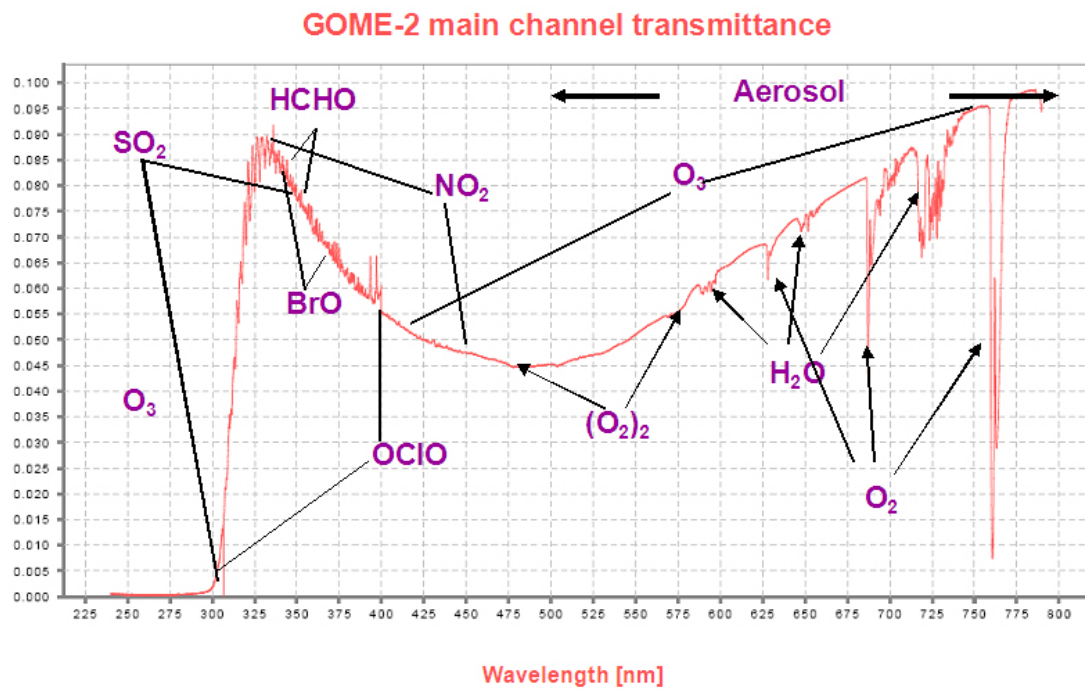


FIGURE 1.9: An example spectrum showing ~~interferences~~ used for species concentration measurements by GOME-2. Image by [EUMETSAT and ESA \(EUMETSAT 2015\)](#).

gives us another way to estimate large scale isoprene emissions, and their subsequent chemistry. How this is performed in this thesis is described in section 3.2.

1.5 Atmospheric Chemistry Modelling

Models can fill the gaps (both spatial and temporal) in measurement records, and can help us improve our understanding of the natural world. They are used to examine future outcomes resulting from changing ~~our~~ emissions, ~~from small to large scales~~. They can be used to increase measurement accuracy (for instance in satellite measurements) and determine where we lack information, while also ~~checking~~ the performance of new instruments. Precisely representing various chemicals and reactions in the atmosphere allows efficient mitigation of pollution, since we can compare scenarios against one another. Models can be expanded to include new compounds or processes, however validation is always necessary. Currently, models require improved isoprene emissions and subsequent chemistry ~~understanding~~ for effective air quality determination (Marvin et al. 2017).

1.5.1 Box models

Box models simulate chemistry in a singular set of conditions without transport or ~~any~~ spatial gradients. These models often parameterise things such as transport and emissions that would realistically take place at the edges of the box. Box models can

be used to check chemical mechanisms in specific scenarios, such as high or low NO_x environments. For example, Marvin et al. (2017) use a box model matching conditions in southeast USA to evaluate isoprene mechanisms from several models.

By allowing for interactions between boxes this concept can be extended to multiple-box models. Multiple-box models are simply multiple instances of single boxes with the addition of transport between them. Transport requires meteorological fields such as wind velocities and turbulence. The meteorology fields can be modelled, and/or input as parameters.

1.5.2 Chemical transport models

Chemical transport models (CTMs) provide a simulation of chemical densities and transport over time, through the atmosphere. Chemistry in the atmosphere is a complex system of coupled reactions and dynamics, which can be solved using numerical partial differential equation solvers. Chemical models require many inputs (such as wind velocities) in order to accurately represent scenarios or regions on earth. Initial (atmospheric starting state) and boundary (inputs and outputs at the edge of the modelled system) conditions are required, and models or inventories of emissions often make up inputs at the surface of the atmosphere.

CTMs simulate production, loss, and transport of chemical species. This is generally calculated using one or both of the Eulerian (box) or Lagrangian (puff) frames of reference. Eulerian models use equations of chemistry within and transport between volumes in a gridded spatial coordinate system, while Lagrangian models look at behaviour within a potentially changing frame of reference (for example within a cloud). CTMs normally solve continuity equations simultaneously for many coupled species. The continuity equations describe transport of a conserved quantity such as mass or energy, which, solved together with production and loss of a chemical can provide detailed simulations of natural processes.

The general continuity equation links a quantity of a substance (q) in the field in which it flows and can be described by the formula:

$$\frac{\partial \rho}{\partial t} + \nabla \cdot j = \sigma$$

where ρ is density of q in the field, t is time, ∇ is divergence, j is the flux (q per unit area per unit time entering or leaving the field), and σ is the generation or loss of q per unit volume per unit time.

The type of model best suited to modelling the entire earth uses the Eulerian frame of reference, where the atmosphere is broken up into 3-D boxes with densities and transport calculated and stored for sequential steps in time at each location. The mass balance equation must be satisfied in any realistic long term model and is as follows:

$$\begin{aligned}\frac{dm}{dt} &= \sum \text{sources} - \sum \text{sinks} \\ &= F_{in} + E + P - F_{out} - L - D\end{aligned}$$

where m is mass of a chemical, E and D are emission and deposition, P and L are production and loss, and F is chemical transport in and out, as shown in figure 1.10.

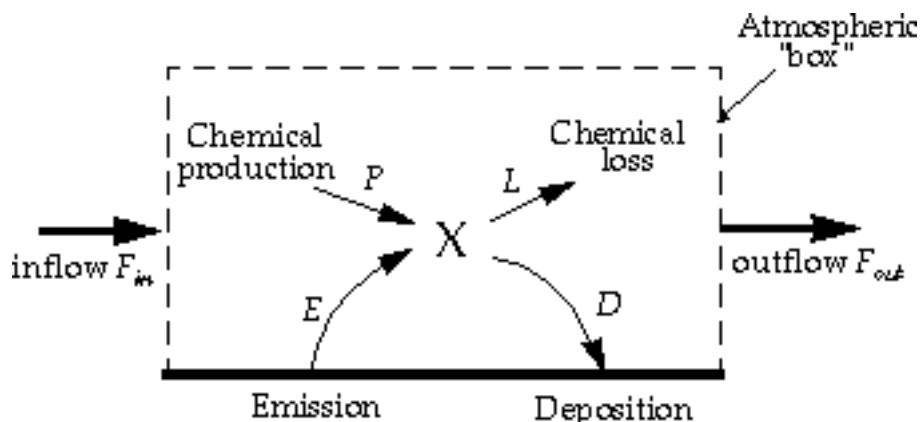


FIGURE 1.10: Standard box model parameters, [image taken](#) from Jacob (1999).

Many chemical species interact with each other through production and loss. Any large chemical model will solve this mass balance equation over highly coupled arrays of partial differential equations, which becomes computation [time](#) expensive as complexity increases.

Contemporary models generally use mathematical differential solving tools of various complexity (often called chemical mechanisms) to solve chemical equations in order to predict chemical species evolutions over time. Different solvers may be slower or faster, and some are more suited to particular situations. The choice of chemical mechanism is normally driven by the mathematical properties of the equations and systems being modelled (such as stability and stiffness), as well as limitations around processing power. Grouping together subsets of model equations or chemical species is often performed and it is possible to use different solvers on each grouping. For example, since $[O] \ll [O_3]$ the chemical family O_X ($O_X \equiv O + O_3$) can be used to simplify chemistry simulations and approximate O_3 concentrations (Brasseur and Jacob 2017, Chapter 3). Different chemical mechanisms may find different solutions to the same problems, due to how the numerical solvers are implemented, which can affect model output (Zhang et al. 2012).

1.5.3 Emissions

There are two commonly used techniques for estimating isoprene emissions, top-down or bottom-up. Bottom-up emission estimates generally model the flora that emit isoprene, along with the rates of emissions and things that affect these rates. The general formula governing modelled emissions E for a species i (from Brasseur and Jacob (2017)) is as follows:

$$E_i = A \times EF_i \times S_i$$

with A the activity rate (eg. how many trees in an area), EF_i being the emission factors (eg. isoprene emitted per tree per year), and S_i is a scaling factor accounting for meteorology and other effects not included in A or F (eg. seasonal temperature).

Isoprene is emitted by trees and shrubs, how much depends on several parameters such as leaf area index (LAI), plant functional type (PFT), and light density fraction.

Models use these properties of the emitters in order to estimate how much isoprene is being produced (eg. Guenther et al. 1995; Guenther et al. 2006). Understanding how much isoprene is emitted, when and by what, is complicated. One frequently used bottom up emissions model is the Model of Emissions of Gases and Aerosols from Nature (MEGAN, Guenther et al. (1995)). MEGAN has estimated $\sim 1150 \text{ Tg C yr}^{-1}$ BVOC emissions globally, of which $\sim 465\text{--}500 \text{ Tg C yr}^{-1}$ is isoprene (Guenther et al. 2006; Messina et al. 2016). In Australia, not much data exists with which to verify these bottom-up emission inventories. Global emissions inventories like MEGAN often have emissions over large areas which are based on extrapolations, which introduces uncertainties (Miller et al. 2014).

Bottom up models of VOC emissions are sensitive to the parameters that drive the emissions. For example, in Asia, isoprene emissions changed by a factor of 2 when temperature, plant type emission factors, incoming solar radiation (insolation) intensity, and land use changes are constrained by measurements (Stavrakou et al. 2014). Sensitivity to these factors is pervasive in bottom up emissions models (eg. Marais et al. 2014; Miller et al. 2014; Messina et al. 2016). One of the important uncertainties seen in MEGAN is the isoprene emissions due to PFTs. If one plant species is emitting heavily near a measuring instrument, possible overestimations may occur due to extrapolation over the entire forest. Current emissions estimates require more validation against observations (Messina et al. 2016). The most important parameters dealing with VOC emissions are LAI, EF, PFT, and light density fraction, with LAI and EF requiring global scale measurements while PFTs and light density fractions require improved parameterisation (Messina et al. 2016).

1.5.4 Uncertainties

This section ~~lists and~~ summarises the major uncertainties models have in relation to VOCs~~s~~ and ozone. Atmospheric chemical models by necessity use simplifications of real world processes, and also utilise information that may be itself uncertain or extrapolated. Uncertainty is introduced through both of these channels as well as through computational limitations, ~~which may be calculating large non-linear non-continuous systems~~.

The concentration of NO_x is an important factor in determining the yield of HCl and ozone from BVOCs. Modelled surface ozone may be overestimated if NO_x emissions are too high, due to their affects on the oxidative capacity of the atmosphere (Travis et al. 2016). NO_x and isoprene emissions ~~are~~ shown to be the most significant sources of uncertainty for ozone concentrations near the surface in GOES-Chem over the US, while isoprene derived products and lightning NO_x drives uncertainty in the upper atmosphere (Christian, Brune, and Mao 2017).

1.5.4.1 Emissions Inventories

Model results can be greatly affected by the choice of emissions inventory used to provide boundary conditions. Natural (biogenic or pyrogenic) and ~~human driven anthropogenic~~ emissions often drive a large fraction of atmospheric oxidation and radical chemistry, especially in the continental boundary layer. Emissions inventories have been found to be generally ~~OK~~ ~~larger~~ (regional to global) scales, as long

as they are derived from accurate input measurements (Zeng et al. 2015). Modelled ozone concentrations have been found to be most sensitive to isoprene emissions and NO_x sources, both of which have uncertain within approximately a factor of 2 (Christian, Brune, and Mao 2017).

Many estimates of isoprene emission are based on a few algorithms that can depend greatly on input parameters (Arneth et al. 2008; Niinemets et al. 2010). Arneth et al. (2008) argue that this monopoly of emissions estimates may be leading us to an incorrect understanding of isoprene chemistry. More recently, Yue, Unger, and Zheng (2015) have shown that this is still a problem, with models of land carbon fluxes showing high sensitivity to VOC emissions. Models which depend on VOC emissions acquire the same sensitivities to light and temperature parameterisations (Yue, Unger, and Zheng 2015).

1.5.4.2 Resolution

Atmospheric chemistry simulations are somewhat sensitive to the gridbox resolution. Reducing model resolution can increase OH concentrations and ozone production rates (Wild and Prather 2006). Increasing model resolution can also impact OH, HO_2 , and ozone concentrations (e.g. Christian, Brune, and Mao 2017). Yu et al. (2016) show how only at higher resolution (0.25 by 0.3125°) does isoprene oxidise under the correct NO_x scheme (through high or low NO_x pathways, see Section 1.3.3.1) in variable NO_x environments. This leads to an increase of high NO_x pathway oxidation of isoprene at the lower resolutions, which leads to an overestimation of HCHO but not ozone at coarser resolutions. However, for many global scale analyses, errors from resolution are less important than those from chemistry, meteorology, and emissions (Christian, Brune, and Mao 2017; Christian et al. 2018).

1.5.4.3 Chemistry mechanisms

Isoprene mechanisms in several contemporary models (including GEOS-Chem) are likely inadequate (Marvin et al. 2017), with changes to reaction rates being inadequate to fix discrepancies from measurements. However, models lack in-situ measurements with which to verify their chemical mechanisms. Often HCHO is used as a way of checking if precursors are correctly modelled since HCHO measurements are more readily available (for instance from satellites). Ozone uncertainties are also affected by inadequate mechanisms, with GEOS-Chem ozone concentrations most sensitive to NO_2 photolysis, the $\text{NO}_2 + \text{OH}$ reaction rate, and precursor emissions (Christian, Brune, and Mao 2017).

1.5.4.4 Clouds

One of the major uncertainties in chemical, climate, radiation, and weather model is cloud formation and dynamics. Clouds are remarkably complex at a much finer scale than can be accurately modelled by global chemistry models (with current processing power). Globally over half (50-60%) of the world is covered by clouds, with ~ 10% of them being rain-clouds (Kanakidou et al. 2005). Wet scavenging performed

in clouds not only depends on large scale cloud processes, but also on the micro-physics of aerosols being scavenged.

1.5.4.5 Soil Moisture

Modelled emissions are sensitive to soil moisture, especially near the wilting point, below which trees stop emitting isoprene and other VOCs completely as they can no longer draw water (Bauwens et al. 2016). MEGAN accounts for soil moisture through a parameterisation that drops plant emissions to zero below a prescribed soil moisture level (the wilting point). Recently an update to this has been shown to improve modelled isoprene emissions in drought conditions (Jiang et al. 2018). Jiang et al. (2018) found that improving the parameterisation of drought based on a measurement campaign in the U.S. would lower isoprene emissions globally by ~ 17%. Many environmental parameters are affected by soil moisture, which all play a role at fine scales to surface emissions (Rowntree and Bolton 1983, Chen and Dudhia 2001). Droughts effects can be difficult to measure, as they are a multi-scale problem that affects various aspects of the land-air interface including plant emissions and dry deposition (Wang et al. 2017).

1.6 Australia and the southern hemisphere

Australia is unique, with its climate, soil moisture, clay content and many other important properties that affect VOC emissions. These properties are only sparsely measured in Australia. Many areas are difficult or expensive to reach, and measurement campaigns are limited. In Australia, most long term air quality or composition measurements are performed in or near large cities. Australia is dominated by areas with little anthropogenic influence, and few ground based measurements of natural emissions take place (VanDerA et al. 2008). Since many Australian cities are on the edge of regions with rich VOC emissions, it is very important to clarify the quantity, type, and cause of VOC emissions. Understanding of emissions from these areas is necessary to inform national policy on air pollution levels.

The vegetation in Australia is diverse, a summary is provided by ABARES using the national forest inventory at <http://www.agriculture.gov.au/abares/forestsaustralia/australias-forests>. Figure 1.11 shows the different forest types and their locations within Australia, highlighting that much of our forested lands are near population centres along the east coast. 16% of Australia is covered by forest, most (75%) of which is Eucalyptus.

Ozone enhancements above the background levels are most sensitive to emissions (of precursor gases), with meteorology, and atmospheric composition also important. Anthropogenic emissions of ozone precursors are important but relatively stable, while pyrogenic sources are greatly variable and dependent on weather, fuel, and fire intensity (e.g. Lawson et al. 2017). Emissions from burning include a range of chemical compounds and particulates and each year the effects of fire or burning seasons blanket the northern and southern hemispheres independently. Biomass burning in southern Africa and South America has previously been shown to have a major influence on atmospheric composition in Australia (Oltmans et al. 2001; Gloudemans et

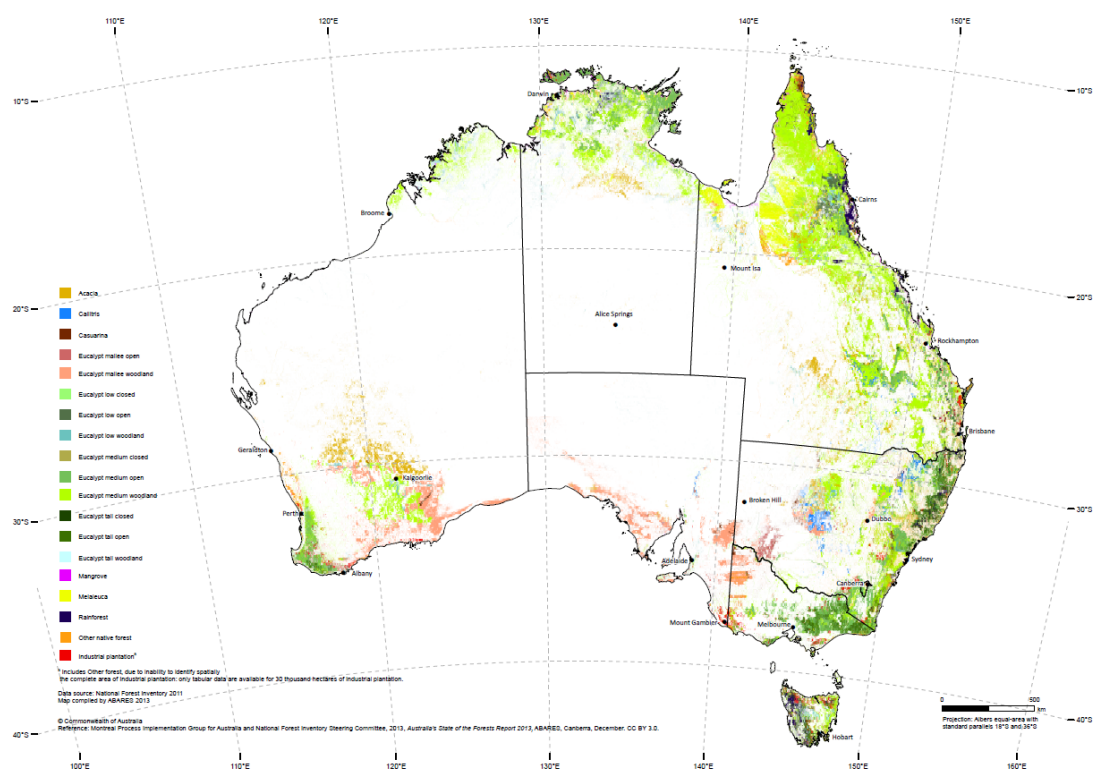


FIGURE 1.11: Forest types in Australia (<http://www.agriculture.gov.au/abares/forestsaustralia/australias-forests>)

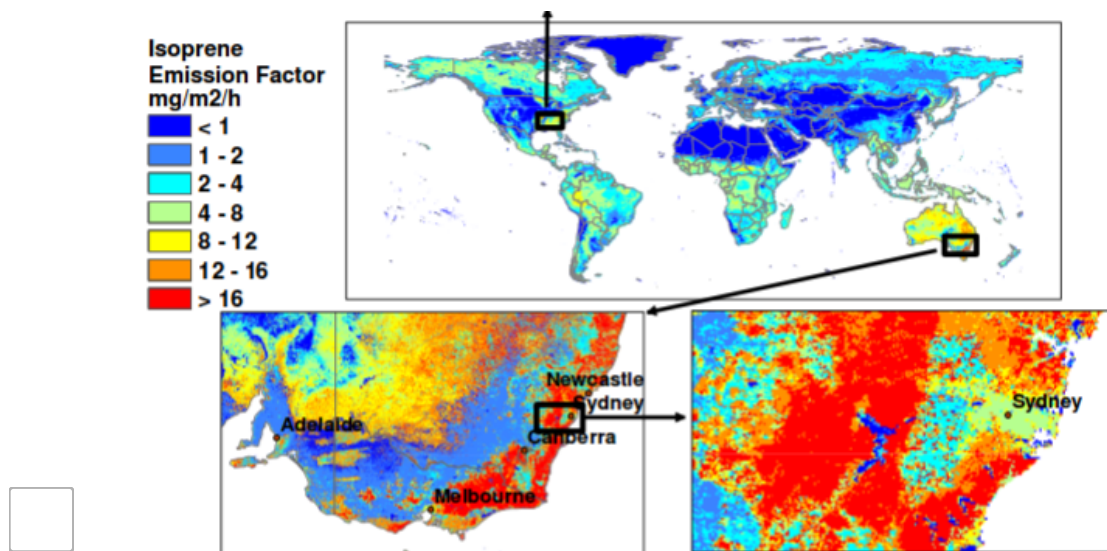


Fig. 2. Global distribution of landscape-average isoprene emission factors ($\text{mg isoprene } \text{m}^{-2} \text{ h}^{-1}$). Spatial variability at the base resolution ($\sim 1 \text{ km}$) is shown by regional images of the southeastern U.S. and southeastern Australia.

FIGURE 1.12: Part of a figure from Guenther et al. (2006) showing global isoprene emission factors.

al. 2006; Edwards et al. 2006), particularly from July to December (Pak et al. 2003; Liu et al. 2016a). Local fires are even more influential and the burning season for Australia can be all year, with severity depending on regional vegetation, recent and current weather, and El-niño.

It has been estimated by MEGAN that the Australian outback is among the world's strongest isoprene emitters, with forests in SE Australia having emission factors greater than $16 \text{ mg m}^{-2} \text{ h}^{-1}$ (see figure 1.12) (Guenther et al. 2006; Guenther et al. 2012). Measurement campaigns in SE Australia have since cast doubt on the emission factors used by MEGAN, potentially due to poor characterisation of Eucalyptus trees and soil moisture (Emmerson et al. 2016; Emmerson et al. 2019). These emissions factor estimates are not well verified and measurements of isoprene (or other BVOC) emissions are sparse and infrequent in Australia (Sindelarova et al. 2014; Bauwens et al. 2016).

1.6.1 Ozone

Surface ozone levels over Australia are relatively low ($\sim 20 \text{ ppb}$) (Young et al. 2017), however it remains unclear how much we would expect this to change in the future as relatively little is known about precursors and influx for the continent. Australian air quality is monitored independently within each state, using several metrics and varying numbers of monitoring stations. Measurement stations are generally located in population centres, and do not regularly measure isoprenoid emissions. This is an important omission as these naturally emitted precursor gases often get transported into cities where they affect air quality through production of O_3 and other pollutants.

Generally STT of ozone over Australia only affects the upper troposphere; however, ozone enhancements can reach quite low during heavy storms and cyclonic

weather patterns (Alexander et al. 2013). The contribution of STT to overall tropospheric ozone budgets remains uncertain, especially in the southern hemisphere (SH) (Škerlak, Sprenger, and Wernli 2014). STT can enhance surface ozone concentrations above legal air quality limits (e.g. Lelieveld et al. 2009; Lin et al. 2015). Detecting ozone enhancements over the background profile in the relatively clean southern ocean atmosphere is simple. However, measurements of ozone over this region are relatively sparse (Škerlak, Sprenger, and Wernli 2014), and quantification of transported ozone is difficult without large scale extrapolations. Ozone enhancements over the southern ocean signify either transported pollution or stratospheric influx (Jacobson and Hansson 2000). Quantifying ozone processes over the southern ocean could improve our understanding of chemistry in the “clean background environment”, while additionally helping to validate model and satellite datasets.

1.6.2 Biogenic VOCs

Bottom up inventories of biogenic VOCs (BVOCs) remain largely uncertain due to missing or extrapolated plant functional type information, changing land cover, and parameterised environmental stressors (Guenther et al. 2000; Karakidou et al. 2005; Millet et al. 2006). Isoprene is one of the most important BVOCs, and is poorly captured by MEGAN (Müller et al. 2008; Sindelarova et al. 2014; Emmerson et al. 2016). Australia has a much greater diversity of tree species than is represented by MEGAN, however sparse measurements of emissions and BVOC concentrations makes model improvement difficult. The complex and parameter sensitive reactions involved in BVOC emissions and subsequent chemistry make model validation even more valuable in this area. Uncertainties in isoprene emissions could explain why models of HCHO over Australia are poor at reproducing satellite measurements (Stavrakou et al. 2009). Improved parameterisation of the effect of drought on plant emissions could also lower modelled isoprene emissions (Jiang et al. 2018).

Australia suffers from poor characterisation of plant emissions, partly because mission factors are based on northern hemispheric data. Many plant emissions rates have not been published, such as those for any Australian acacias. Some Eucalypt emissions are based on samples from young trees, which may emit more isoprene than older trees (Emmerson et al. 2016). Changes in parameterisation of soil moisture in the MEGAN lead to large reductions (38 – 58%) in Australian isoprene emission estimates, although errors remain (Sindelarova et al. 2014; Emmerson et al. 2019). Over Australia MEGAN suffers from a lack of studied plant functional types and their emissions (eg. Müller et al. 2008). Emission rates from various species of Eucalyptus and other flora are highly complex, depending on current and recent weather, temperature, tree age, health, etc. (Guenther et al. 2012).

Other than satellite data, four independent data sets are used in this thesis: FTIR on the roof of the Wollongong university chemistry building, MUMBA, SPS1 and SPS2 (see Section 2.2). These measurements take place in south eastern Australia, and have suggested lower isoprene emissions than seen in models (by a factor of 2-6) (Emmerson et al. 2016). Several improvements are required as no simple scaling factor can completely fix the misrepresentation of isoprene emissions (Emmerson et al. 2016).

Improvements to emissions models require improved understanding of regional vegetation and how this regional vegetation responds to meteorological and chemical

parameters. Satellite measurements of HCHO can be used to estimate and improve Australian isoprene emissions without costly measurement campaigns. This is due to the near-linear link between HCHO and isoprene emissions (e.g., Palmer et al. 2001; Millet et al. 2006; Bauwens et al. 2016).

1.6.3 Measurements

Isoprene and many of its products can be difficult to measure accurately due to their short lifetimes, high reactivity, and optically thin natures. There are relatively few measurements in Australia, including short term campaigns MUMBA (Paton-Walsh et al. 2017), and SPS (Dunne et al. 2018). These measurements focus on air quality and biogenic VOCs and use several different instruments (including PTR-MS and GC-FID) to detect metrics such as air particulates, HCHO, isoprene, and meteorological information. There is also an instrument at Wollongong university (see Section 2.2.3.4) that provides 20 years of HCHO measurements, which is the only available long term HCHO vertical column measurement comparable to satellite data. Satellite HCHO column measurements can be limited by various factors including interfering species, water, clouds, orography, etc, and independent in-situ measurements are required to validate the data. For further details on these campaigns and measurements, see Section 2.2.

Detecting ozone from the surface up to the top of the stratosphere requires different techniques such as remote sensing and ozonesonde releases. Ozonesondes are weather balloons (with attached ozone detectors) that detect ozone concentrations up to the mid stratosphere (~ 30 km), providing a vertical profile over a single location. Since 1986, Lauder, New Zealand (45°S , 170°E) has released ozonesondes allowing a multi-decadal analysis of ozone concentrations over the city (Brinksma et al. 2002).

Kerguelan Island (49.2°S , 70.1°E), also has a record of ozonesonde profiles, which are directly in the path of biomass burning smoke plumes transported off shore from Africa (Baray et al. 2012). SHADOZ is the southern hemispheric additional ozone project, which have released sondes from 15 sites at different times <http://trop.gsfc.nasa.gov/shadoz/>. A smaller network of ozonesonde release sites (including Davis, Macquarie Island, and Melbourne) is available from the world ozone and ultraviolet radiation data centre <http://woudc.org/data/explore.php> and is used in Chapter 4 to examine stratospheric impacts on tropospheric ozone (see 2.2.3.3 for more info on these ozonesondes).

1.7 Aims

In this thesis I aim to improve understanding of natural contributions to ozone over Australia and the southern ocean. The two largest contributors to tropospheric ozone concentrations are chemical production (driven by precursor emissions) and stratospheric transport. I aim to improve understanding of both of these sources using existing satellite and ground-based datasets along with GEOS-Chem modelled outputs.

Estimation of BVOC emissions in Australia can be improved through satellite measurements of HCHO, one of isoprene's primary oxidation products. Satellites that

overpass daily record reflected solar (and emitted terrestrial) radiation, and give us measurements over all of Australia. Combining satellite data with model outputs provides a platform for the understanding of natural processes, which are uncertain over Australia. Satellite measurements ~~use~~ modelled a priori vertical profiles of HCHO to estimate total column amounts. I aim to recalculate satellite vertical columns of HCHO using updated model a priori information. In this effort I aim to improve the understanding of the importance of relevant parameters (within GEOS-Chem) in calculating vertical columns of HCHO measured by satellite. This includes an examination of how well GEOS-Chem simulates several species such as NO_x , isoprene, and HCHO compared to both in-situ and remote measurement data that exists for Australia. Additionally, I detail the construction and effects of satellite data filters. The work towards this aim is in Chapter 2.

The technique of determining isoprene emissions from satellite detected HCHO is called satellite inversion. I aim to determine isoprene emissions in Australia using a top-down inversion of satellite HCHO, through an estimated yield from isoprene to HCHO. HCHO amounts and the yield of isoprene to HCHO over Australia is required to create top-down estimates. This process also requires careful examination of when the assumptions required within the inversion process are not valid. Due to the low availability of in-situ data over most of the Australian continent, a combination of modelled and satellite data ~~could~~ reduce the uncertainties of isoprene emissions from Australian landscapes. Improved emissions estimates will in turn improve the accuracy of CTMs, providing better predictions of atmospheric composition and its response to ongoing environmental change. The work towards fulfilling this aim is in Chapter 3.

I aim to improve understanding of ozone transported to the troposphere from the stratosphere in Australia and the southern ocean. Stratospheric transport is the second largest driver of tropospheric ozone concentrations, and an improved understanding of transported ozone can be determined from ozonesonde measurements. Ozonesondes provide a glimpse of the vertical ozone profile up to ~ 30 km, and we use a Fourier filter to determine how often stratospheric transport is occurring at three sites: Melbourne, Macquarie Island, and Davis Station. Combining transport event frequency analysis with modelled ozone distributions is used to derive a new method of detection and quantification of transported ozone in Chapter 4.

I aim to describe relative importance of sources of tropospheric ozone in Australia, as well as seasonality. I will describe how modelled ozone is affected by updated isoprene emissions, comparing changes in GEOS-Chem outputs. Trends of isoprene emissions and their relationship to tropospheric ozone trends could provide new insight into the future of tropospheric ozone in Australia.